THEMED ISSUE: EarthScope IDOR project (Deformation and Magmatic Modification of a Steep Continental Margin, Western Idaho–Eastern Oregon)

THE GEOLOGICAL SOCIETY OF AMERICA®

Internal fabrics of the Idaho batholith, USA

A. Byerly[1], B. Tikoff[1], M. Kahn[1], B. Jicha[1], R. Gaschnig[2,*], and A.K. Fayon[3]
[1]DEPARTMENT OF GEOSCIENCE, UNIVERSITY OF WISCONSIN–MADISON, MADISON, WISCONSIN 53706, USA
[2]SCHOOL OF EARTH AND ATMOSPHERIC SCIENCE, GEORGIA INSTITUTE OF TECHNOLOGY, ATLANTA, GEORGIA 30332, USA
[3]DEPARTMENT OF EARTH SCIENCES, UNIVERSITY OF MINNESOTA, MINNEAPOLIS, MINNESOTA 55455, USA

ABSTRACT

The Idaho batholith of the North American Cordillera is a large and long-lived silicic intrusive center. We studied fabrics at the regional scale within the different intrusive suites of the Idaho batholith, using microstructural characterization, anisotropy of magnetic susceptibility measurements, and shape preferred orientation analyses. Each studied outcrop was collocated with existing U-Pb zircon geochronology and ongoing (U-Th)/He zircon thermochronology results. Three new $^{40}Ar/^{39}Ar$ biotite ages, collocated with the existing U-Pb zircon ages, constrain the cooling rates within the batholith. The presence of dominantly magmatic microstructures allows us to interpret the results relative to the U-Pb zircon ages and observe spatial and temporal patterns of fabric development. The early (pre–80 Ma) intrusive suites exhibit solid-state microstructures that show a consistent orientation only in the western part of the batholith. Fabrics in the 83–67 Ma Atlanta peraluminous suite are weak and inconsistent in orientation, despite emplacement during regional contraction. We hypothesize that the lack of consistently oriented fabrics in the Atlanta lobe results from either: (1) topographic effects that caused local extensional/neutral strain environments in the upper parts of a crustal plateau; or (2) emplacement in thin, horizontal magmatic sheets. In contrast, fabrics within the 66–53 Ma Bitterroot peraluminous suite are well developed and consistently oriented (NW-striking; NE-dipping), recording localized contraction during magmatism.

LITHOSPHERE; v. 9; no. 2; p. 283–298 | Published online 12 October 2016 doi: 10.1130/L551.1

INTRODUCTION

Large silicic intrusive complexes are fundamental building blocks of the continental crust. Understanding these large intrusive centers is essential to our understanding of the growth and recycling of continental crust. Many workers have evaluated the internal structure of individual plutons as constituent parts of larger batholiths to understand batholith construction and deformation through time (Tobisch et al., 1995; Borradaile and Henry, 1997; Benn et al., 1998, 2001; Launeau and Cruden, 1998; McNulty et al., 2000; Neves et al., 2003; Mamtani and Greiling, 2005; Sen and Mamtani, 2006; Zak et al., 2007; Archanjo et al., 2008; DeCelles et al., 2009; Benn, 2010; Mamtani et al., 2013; Cao et al., 2015; Paterson and Ducea, 2015). This approach of analyzing plutons as discrete, time-successive crustal additions provides insight into the broader magmatic and tectonic regime. Tobisch et al. (1995), for example, used the spatial and temporal distribution of magmatic versus solid-state fabric in the central Sierra Nevada batholith (Fig. 1) to reconstruct the evolution of this Cordilleran magmatic arc. They evaluated deformation within restricted areas and time frames defined by mapped plutonic boundaries. The fabrics, within the framework of known regional-scale plate trajectories and average strain rates, were then used to elucidate the orientation and magnitude of broad-scale tectonic strain. Similarly, Chardon et al. (1999) examined fabrics within compositionally and structurally distinct plutons in the Coast plutonic complex (Fig. 1). These syntectonic plutons record large-scale transpression and together were used to reconstruct the tectonic evolution of shear zones within the broader batholith. Results have shown that the growth and deformation record of batholiths provides magmatic and tectonic constraints that contribute to our understanding of the growth and recycling of continental crust.

Construction of a batholith can be understood by evaluating the growth history of individual plutons. Most granitic intrusions record some fabric, and quantitative evaluation of the macroscopically indiscernible fabrics helps to elucidate the subtle strain recorded during magma crystallization (e.g., Bouchez, 1997). Magmatic fabrics, in particular, preserve orientations and magnitudes that result from the final increment of strain at the time of crystallization (e.g., Marre, 1986; Hutton, 1988; Paterson et al., 1989, 1998; Benn, 2010). The preservation of magmatic microstructures indicates the magmatic fabrics were "locked in" during a limited time interval immediately prior to crystallization (e.g., Fowler and Paterson, 1997; Yoshinobu et al., 1998). By combining microstructural data with U-Pb zircon ages from individual plutons, the regional tectonic activity through time can be assessed.

The majority of the Idaho batholith lacks the typical internal plutonic contacts of other large silicic batholiths in the North American Cordillera (Fig. 1). Common structures in other magmatic arcs—mesoscale folds, kilometer-scale shear zones, mixing and mingling zones—are largely absent in the Atlanta lobe of the Idaho batholith. Rather, these granites are remarkably uniform in composition and structure, consisting primarily of biotite granodiorite and two-mica granite/granodiorite. The recent designation of magmatic suites within the batholith required a combination of geochronology and geochemistry (Gaschnig et al., 2010, 2011). Due to the apparent compositional homogeneity and cryptic structure, little attention has been paid to the tectonic record preserved within the batholith. Because of these factors, evaluating the first-order growth and deformation history of the Idaho batholith requires a different approach

*Present address: Department of Environmental, Earth and Atmospheric Sciences, University of Massachusetts Lowell, Lowell, Massachusetts 01854, USA

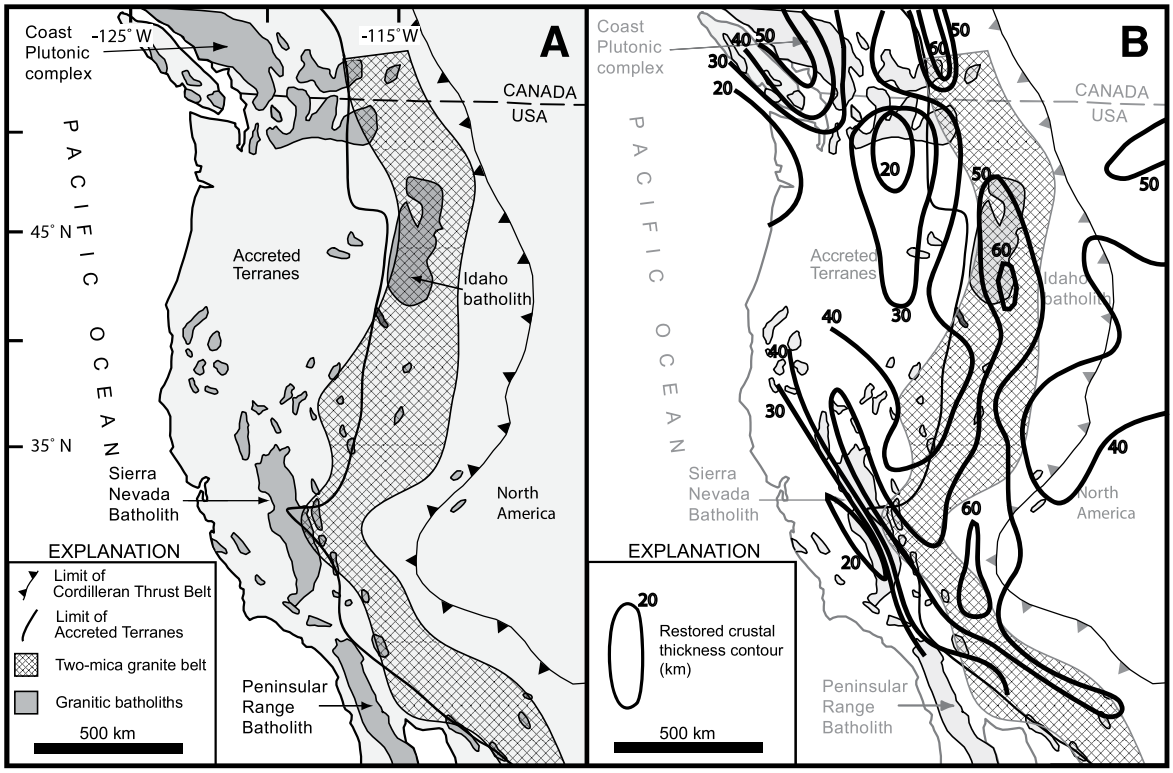

Figure 1. (A) Four large North American Cordilleran batholiths and their spatial relationship to the Sr 0.706 line, the geochemically defined boundary between accreted terranes and cratonic North America (Armstrong et al., 1977). (B) Map of restored crustal thicknesses (Coney and Harms, 1984) superimposed on Late Cretaceous–Paleogene two-mica granite belt (Miller and Bradfish, 1980) showing the spatial coincidence of overthickened crust and the Idaho batholith. Contours are 10 km.

than that applied to the study of other Cordilleran batholiths.

We present fabric measurements of samples from dated (U-Pb zircon; Unruh et al., 2008; Giorgis et al., 2008; Gaschnig et al., 2010, 2013, 2016; Braudy et al., 2016) field sites to reconstruct the fabric evolution of the Idaho batholith through time. By tying structural measurements to geochronologic data, we evaluate the record of deformation preserved within the Idaho batholith at specific time-space points. This approach was chosen for the Idaho batholith because it is not dependent on the *a priori* ability to map individual plutonic boundaries. Fabric orientations and magnitudes were measured using shape preferred orientation (SPO) and anisotropy of magnetic susceptibility (AMS) techniques.

GEOLOGICAL BACKGROUND

The Idaho batholith of the North American Cordillera is a large silicic intrusive center, consisting of the Atlanta lobe in the south and the Bitterroot lobe in the north. The Atlanta lobe, the largest part of batholith, exhibits distinctively homogeneous composition and internal structure (Fig. 2). Gaschnig et al. (2010, 2011) constrained the emplacement and crystallization history and tracked the source and isotopic evolution of the crustal melt. The emplacement of the Idaho batholith and the intrusion of the subsequent Challis suite account for ~32,000 km^2 spatial extent at present, representing a 50 m.y. (98–43 Ma) episode of magmatism.

Prior to Idaho batholith magmatism, a spatially restricted N-S–trending series of plutons forming the suture zone suite of Gaschnig et al. (2010) was intruded in western Idaho, straddling the boundary between cratonic North America and accreted terranes (Manduca et al., 1992, 1993; Giorgis et al., 2008; Gaschnig et al., 2010). The suture zone suite was affected by the western Idaho shear zone, a major transpressional shear zone (e.g., Giorgis et al., 2008).

We utilized the divisions of Gaschnig et al. (2010), who distinguished intrusive suites of the Idaho batholith based on a combination of lithology, geochronology, and geochemistry (Fig. 2). The main phases of the batholith are: (1) the early metaluminous and border zone suites (98–85 Ma); (2) the Atlanta peraluminous suite (83–67 Ma); (3) the late metaluminous suite (75–69 Ma); and (4) the Bitterroot peraluminous suite (66–53 Ma; Gaschnig et al., 2010, 2011). Magmatism continued in Idaho with the Challis intrusive suite (51–43 Ma; Gaschnig et al., 2010, 2011), which is not considered to be part of the Idaho batholith.

The border zone suites consist of a series of N-S–trending tabular bodies located east of the western Idaho shear zone and suture zone plutons. Early metaluminous plutons were emplaced simultaneously with the border zones suite, but they are exposed in the Atlanta lobe of the Idaho batholith as roof pendants and septa within the younger phases and along the eastern boundary of the batholith. The Atlanta peraluminous suite is the largest phase of the batholith, making up the majority of the Atlanta lobe, and it is relatively homogeneous in structure and composition (biotite granodiorite and two-mica granite). Evolved Hf and Nd isotopes and evolved major-element compositions with limited range suggest that magma was derived almost exclusively from preexisting continental crust and received little material input from the mantle (Gaschnig et al., 2011). The Bitterroot lobe consists of a late metaluminous suite (75–69 Ma) and the Bitterroot peraluminous suite (66–53 Ma), and it was initiated during the waning stages of emplacement of the Atlanta

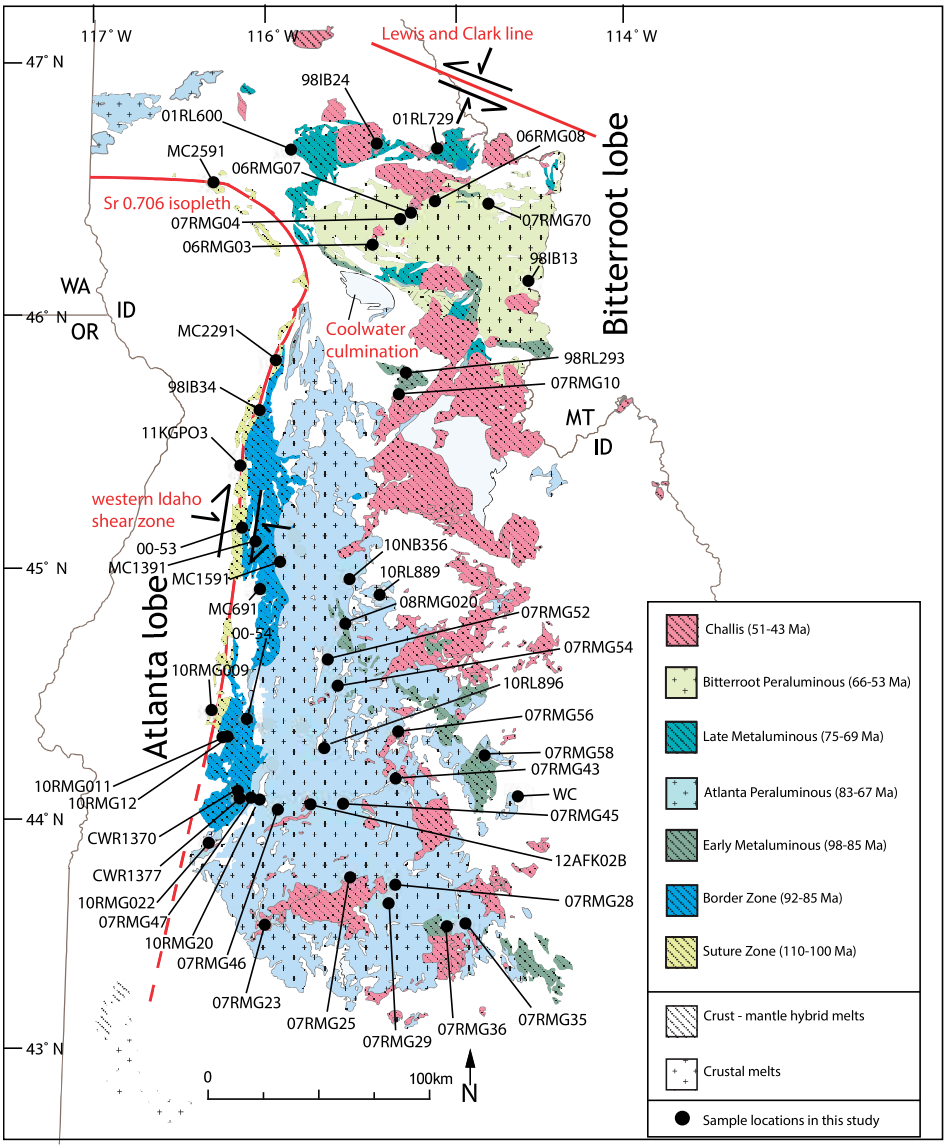

Figure 2. Sample locations used in this study, plotted on the intrusive suites of the Idaho batholith from Gaschnig et al. (2010). The red line shows the position of the Sr 0.706 line, which is typically coincident with the western Idaho shear zone (WISZ). State abbreviations: WA—Washington, OR—Oregon, ID—Idaho, MT—Montana.

peraluminous suite. Finally, the Challis suite (51–43 Ma) is a regionally extensive intrusive and extrusive group that intrudes earlier Idaho batholith granites.

ASSESSING FABRIC DEVELOPMENT IN GRANITIC ROCKS: METHODS AND RESULTS

Background

Fabrics in plutons provide important information about the emplacement and postemplacement deformational history of an igneous body; these fabrics are grouped into magmatic fabrics and solid-state fabrics (e.g., Paterson et al., 1989; Benn et al., 2001; de Saint-Blanquat et al., 2001). Magmatic fabrics form via the mechanical alignment of anisotropic phases in the presence of melt (e.g., Marre, 1986; Paterson et al., 1989, 1998). Fabric development may result from internal (e.g., flow, mixing, thermal convection) or external (regional strain) processes. Previous workers have interpreted magmatic fabrics in plutons as a record of either magmatic processes at the emplacement level (Cruden and Launeau, 1994; Tobisch and Cruden, 1995; Archanjo et al., 1999; Ferré et al., 1999; de Saint-Blanquat et al., 2001, 2006; Parada et al., 2005; Stevenson et al., 2007; Naibert et al., 2010; Archanjo and Campanha, 2012; Gutiérrez et al., 2013; Morgan et al., 2013) or regional strain during syntectonic emplacement (Brun and Pons, 1981; Brun et al., 1990; Archanjo et al., 1995; Leblanc et al., 1996; Benn et al., 1997, 1999, 2001; Sen et al., 2005; Mamtani et al., 2013). Solid-state (or subsolidus) fabrics in granitic intrusions are formed by crystal-plastic deformation of phases in the absence of melt. Solid-state fabrics in granites are generally used to track distributed regional-scale strain and to document kinematics of localized shear zones. In some cases, solid-state fabrics are used to infer synemplacement deformation, such as the deformation of a marginal facies of an intrusion by an internal facies (e.g., de Saint Blanquat et al., 2001). Solid-state fabrics superimposed on magmatic fabrics represent an overprinting of emplacement-level processes (e.g., Gleizes et al., 1998; Pignotta and Benn, 1999; Zak et al., 2007) or time-transgressive tectonic fabrics in a cooling pluton (e.g., Bouchez et al., 1990; Karlstrom et al., 1993; Aranguren et al., 1996; Mamtani and Greiling, 2005; Baxter et al., 2005; Henry et al., 2009; Majumder and Mamtani, 2009; Sant'Ovaia et al., 2010).

In the case of magmatic deformation, granites provide superb evidence for the timing of fabric development. Igneous rocks that contain >5% melt during cooling are significantly weaker than fully crystallized rocks (e.g., Vigneresse and Tikoff, 1999; Mecklenburgh and Rutter, 2003; Rosenberg and Handy, 2005). Thus, deformation preferentially partitions into semimolten igneous rocks. In contrast, once a granitic body has crystallized, it is typically competent relative to other sedimentary and metamorphic rock types (e.g., Paterson et al., 1989). Thus, magmatic fabrics can be used to infer deformation related to either emplacement processes or regional deformation during a limited time interval following emplacement and prior to complete crystallization. If both the crystallization age of the granite and a cooling history are known, the history of deformation can be constrained.

Sampling and Field Fabrics

Samples were collected from field sites that had previously been dated using U-Pb on zircon (Unruh et al., 2008; Giorgis et al., 2008; Gaschnig et al., 2010, 2013; Braudy et al., 2016). Field-based fabric within the Idaho batholith is often very subtle; foliations were observed at some locations, and lineations were not observed except in the border zone suite. Field-based magmatic foliation throughout the Idaho batholith is defined by the alignment of biotite and, locally, potassium feldspar. In contrast, solid-state foliations are defined by elongate quartz in addition to aligned biotite.

Microstructures

Microstructural Characterization and Classification

The three categories of microstructures in this study are: (1) magmatic; (2) slight solid-state overprint; or (3) solid state. This classification follows from other studies in which microstructures have been used qualitatively to document the conditions of deformation (e.g., Paterson et al., 1989; Bouchez et al., 1990; Bouchez and Gleizes, 1995; Mamtani and Greiling, 2005; Benn, 2010; Sant'Ovaia et al., 2010). A detailed list of microstructural observations for all samples in this study is given in Byerly (2014).

Criteria for magmatic microstructures include: (1) quartz grains that are consistently coarse grained, anhedral with relatively straight grain boundaries, and lack subgrains; (2) alkali and plagioclase feldspar grains that are coarse grained and pervasively exhibit growth twins; and (3) biotite grains that are undeformed and distributed throughout the sample.

The slight solid-state overprint microstructure contains magmatic microstructures, but it also includes some of the following subsolidus microstructures: undulatory extinction of quartz, bulging or interlobate grain boundaries, quartz-filled fractures in feldspar, and deformation twins in feldspar (Blumenfeld and Bouchez, 1988; Paterson et al., 1989). Quartz grains are large and equant, but grain boundaries are bulging rather than straight. Carlsbad growth twinning is preserved in plagioclase feldspar, and tartan twinning is preserved in alkali feldspar. The lack of a well-developed SPO in these samples suggests that solid-state overprinting was minimal.

Criteria for solid-state microstructures are primarily based on the size, shape, and structure of quartz. Quartz microstructures include elongate grains that define a consistent SPO, pervasive undulatory or checkerboard extinction, a bimodal grain-size distribution, and bulging and interlobate grain boundaries. Larger quartz grains are mantled by small, recrystallized grains; quartz also displays subgrains. Solid-state deformation is also evidenced by the presence of kinked biotite grains and deformation twins in plagioclase feldspar grains. Though these microstructures all reflect solid-state strain, they formed at a range of temperatures. For instance, medium- to high-temperature (400–700 °C) solid-state deformation is inferred from checkerboard extinction and anisotropic quartz grains due to recrystallization by subgrain rotation and grain boundary migration (Hirth and Tullis, 1992; Lloyd and Freeman, 1994; Stipp et al., 2002), whereas bulging quartz grain boundaries and patchy undulatory extinction can form at significantly lower temperatures (~300–400 °C; e.g., Stipp et al., 2002).

Observed Microstructures

The U-Pb zircon crystallization ages provided by Unruh et al. (2008), Giorgis et al. (2008), Gaschnig et al. (2010, 2013), and Braudy et al. (2016) allow us to evaluate these microstructural observations within a temporal framework, which is added to the spatial framework given by the distribution of the samples. We discuss each magmatic suite, from oldest to youngest (border zone, early metaluminous Atlanta suite, late metaluminous, Bitterroot suite), to elucidate the tectonic history of magmatism in the Idaho batholith.

Samples from the border zone and early metaluminous suites exhibit both a magmatic and slight solid-state overprint or solid-state fabrics (Fig. 3). Feldspar grains commonly exhibit deformation twinning and anhedral morphology. Biotite locally defines a SPO and is found in aggregates. Foliations are NS-to-NNE striking, parallel to the regional trend of the western Idaho shear zone. Samples from the early metaluminous suite locally show strong fabric development, but the directions are not regionally consistent.

The Atlanta peraluminous suite preserves dominantly magmatic microstructures (Fig. 3). Grain size is commonly coarse, with blocky grains, suggesting that the original magmatic microstructure is preserved. Though some quartz grains have serrated grain boundaries and undulatory extinction, they are generally equant and sometimes preserve 120° triple junctions. Alkali feldspar is commonly subhedral and blocky with tartan twinning, and oscillatory zoning is found in many plagioclase feldspar grains. Mica is distributed throughout samples, and the mica cleavage is rarely kinked or fractured. The Atlanta peraluminous suite locally records slight solid-state overprint, but there is no trend in the spatial distribution. We interpret fabric preserved in the rocks of the Atlanta peraluminous suite to represent fabric acquired in the magmatic state, immediately before full crystallization.

Solid-state microstructures were identified in the Bitterroot peraluminous and late metaluminous suites, indicating that magmatic microstructures were modified or obliterated by subsolidus deformation. Quartz in samples from this suite commonly displays undulatory or checkerboard extinction, is occasionally dynamically recrystallized, and in extreme cases is elongate and defines an SPO (Fig. 3). Alkali feldspar is commonly subhedral to anhedral and occasionally fractured. Plagioclase feldspar often displays deformation twins (Fig. 3). In samples with a weak solid-state overprint (e.g., 06RMG03), magmatic microstructures still dominate. In samples with strong solid-state fabric (e.g., MC25-91), subsolidus microstructures dominate, and any fabric formed prior to crystallization has been drastically altered or obliterated.

SHAPE PREFERRED ORIENTATION

Methodology

These weak and dominantly magmatic fabrics, as characterized in the previous paragraphs, were quantified by SPO. Fabric in intrusive rocks can be defined by the alignment of minerals, alignment of mineral aggregates, deformed phases such as quartz ribbons, or deformed markers such as enclaves. Fabric in rocks that preserve original igneous texture is defined by the early crystallizing phases, which are able to rotate into alignment in the presence of melt. In the Idaho batholith granites, fabrics are generally defined by aligned biotite.

The method of SPO analysis provides a quantitative fabric orientation, shape, and strength for each sample. Orientation is given by a fabric ellipsoid with axes K1 ≥ K2 ≥ K3 that defines the lineation (long axis = K1) and the pole to the foliation (short axis = K3) in a geographic reference frame. The shape of the fabric is defined by the shape parameter, $T = \{(\log[K2/K3] - \log[K1/K3])/(\log[K2/K3] + \log[K1/K2])\}$, which ranges from −1 (prolate) to 1 (oblate), representing constrictional or flattening deformation, respectively (Jelinek, 1981). The strength of fabric is defined by the degree of anisotropy, $P' = (K1/K3)$. Because all intrusive suites in the Idaho batholith contain biotite, this phase was used as the basis for SPO comparison.

Three mutually perpendicular thin sections were prepared for 46 samples. Each sample was oriented in the geographic coordinate system: one horizontal face, one north-striking vertical face, and one east-striking vertical face. Each thin section was photographed using a digital camera attached to a microscope. Biotite was isolated in binary images using ImageJ (National Institute of Health's public domain image processing software). These thin sections were also compared to unoriented thin sections used during earlier geochronological-based studies (Gaschnig et al., 2010; Braudy et al., 2016).

Binary images of biotite grains were analyzed using Patrick Launeau's SPO2003 and Ellipsoid2003 software, utilizing the intercept method (Launeau et al., 1990; Launeau and Robin, 1996). The intercept method is used for determining the alignment of phases within a series of mutually perpendicular two-dimensional planes, which are then combined into a three-dimensional ellipsoid. The number of intercepted grain boundaries is counted along a set of parallel scan lines that are rotated around the image by a specified angular increment. The

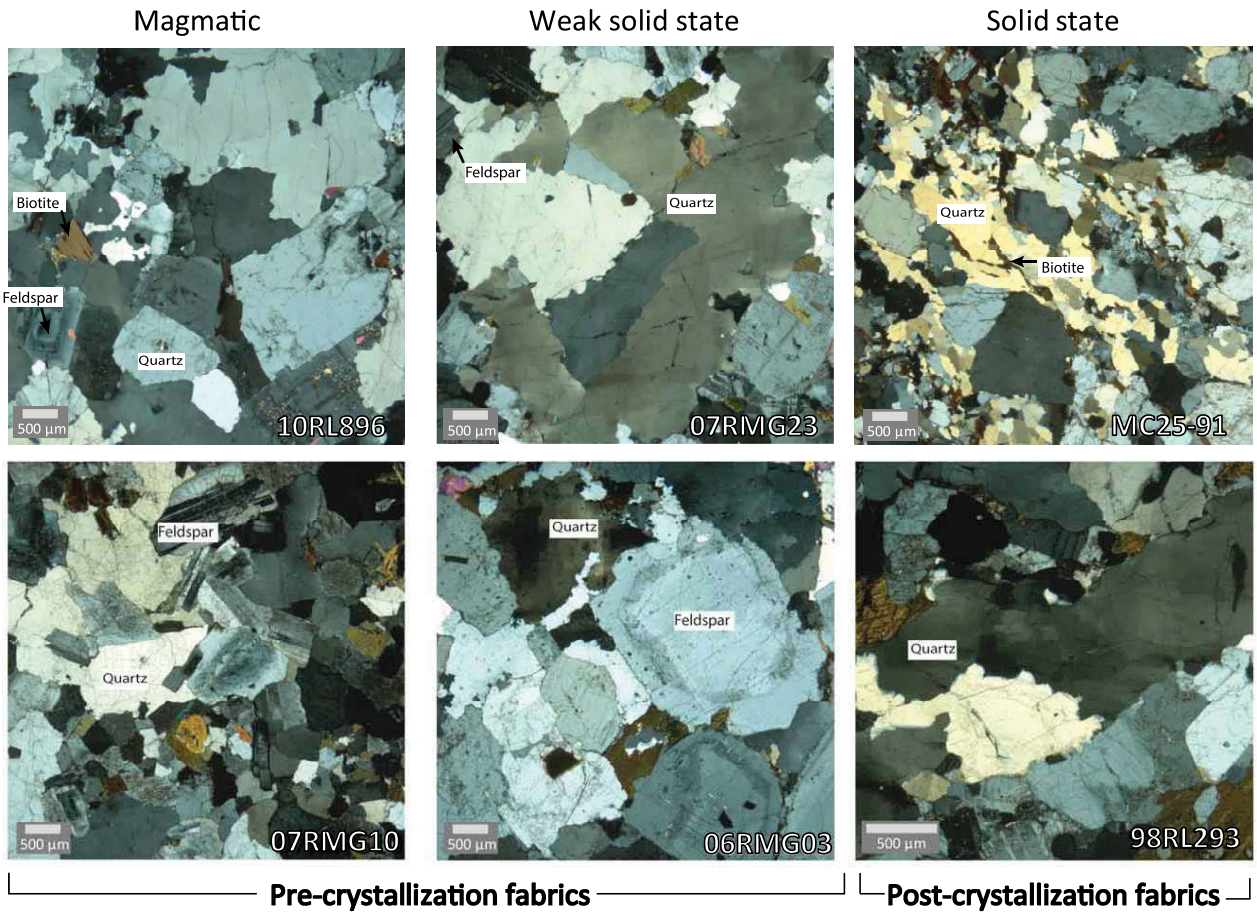

Figure 3. Representative microstructures in the Idaho batholith. Left: Magmatic microstructures include coarse-grained, roughly equant quartz, and both growth twins and concentric zonation in feldspar. Center: Samples with weak solid-state overprint show similar characteristics to magmatic microstructures, but with some interlobate grain boundaries and undulatory extinction. Right: Solid-state microstructures include elongate quartz grains with undulatory extinction, subgrains, and recrystallized grains.

direction in which these intercept counts is the lowest is the direction of preferred orientation. The aggregate preferred orientation of grains is averaged to determine the average SPO within a given thin section. SPO2003 analyzes the inertia and intercept tensor of each thin section individually, producing a two-dimensional ellipse that quantifies the fabric strength and orientation for the phase of interest. The three ellipses from the different faces of each sample are combined into a three-dimensional ellipsoid using Ellipsoid2003. The result is an average fabric ellipsoid that can be characterized for each sample by orientation, shape, and degree of anisotropy.

Results

The results of SPO analysis of biotite suggest weak fabrics with a wide range of fabric shapes. The degree of anisotropy (P′) of SPO fabrics determined using the intercept method ranges from 1.03 to 1.23, with an average of 1.09, or 9%. There is a wide range of SPO fabric shapes represented, with a range in shape parameter (T) from –0.85 to 0.83 (Byerly, 2014). Figure 4 indicates that there is no correlation between degree of anisotropy and shape parameter.

SPO fabric orientations are generally parallel to fabrics measured in the field, and they show some regional patterns (Fig. 5). The plutons of the suture zone suite record the mylonitic fabric of the western Idaho shear zone, which is a consistently north-striking foliation that dips steeply to the east. SPO foliations of the border zone suite also strike north and dip steeply to the east. The early metaluminous plutons on the eastern and northern borders of the Atlanta lobe show no consistent trend in SPO foliation or lineation orientation. The degree of anisotropy for fabrics determined using the intercept method ranges from 1.06 to 1.23. SPO fabrics are prolate to oblate: The shape parameter ranges from –0.85 to 0.78.

The Atlanta peraluminous suite exhibits highly variable fabric strength, shape, and orientation (Fig. 5). SPO foliation and lineation within the Atlanta peraluminous suite have no

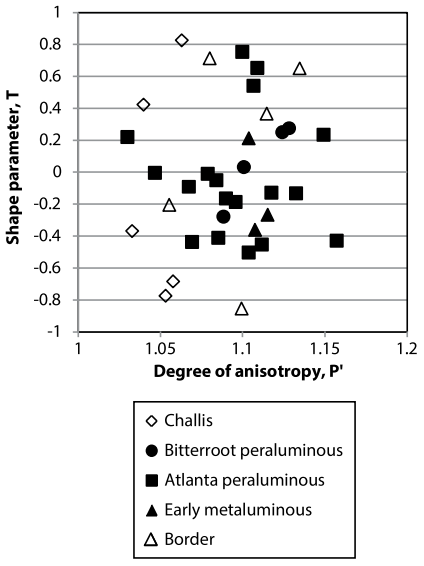

Figure 4. Results of shape preferred orientation (SPO) analyses. Plot of shape parameter (T) vs. degree of anisotropy (P′), indicating no correlation between the fabric strength and shape parameter.

consistent trend in orientation. The degree of anisotropy for fabrics determined using SPO ranges from 1.03 to 1.16. Fabrics are dominantly prolate in shape, with a range in T of −0.5 to 0.75. Both the strength and shape of SPO fabrics are variable through time, showing no clear trend through the 16 m.y. of Atlanta peraluminous magmatism.

Foliations in the Bitterroot lobe strike NNW and dip moderately to the NE, parallel to those measured in outcrop. Lineations are consistently subhorizontal. The degree of anisotropy for fabrics determined using SPO ranges from 1.08 to 1.12. Fabrics are dominantly weakly oblate, with shape parameter values from −0.28 to 0.28.

ANISOTROPY OF MAGNETIC SUSCEPTIBILITY (AMS)

Methodology

Magnetic susceptibility is a dimensionless proportionality defined as the ratio of the magnetization induced in a sample to the strength of the applied field (e.g., Hrouda, 1982). Susceptibility is commonly directional, and AMS is a second-rank tensor that can be represented by an ellipsoid. The AMS ellipsoid has three mutually perpendicular axes, where K1 ≥ K2 ≥ K3. The long axis, K1, represents the magnetic lineation, and the short axis, K3, is the pole to the magnetic foliation. The orientation, shape, and strength of the magnetic susceptibility ellipsoid (AMS ellipsoid) serves as a proxy for petrofabric measurements (Jelinek, 1981; Hrouda, 1982; Tarling and Hrouda, 1993; Bouchez, 1997; Borradaile and Jackson, 2004) because magnetic axes of common paramagnetic and ferromagnetic phases are parallel to shape axes. Bulk susceptibility (K1 + K2 + K3)/3 varies by orders of magnitude depending on the class of magnetic material (e.g., diamagnetic, paramagnetic, and ferromagnetic, in order of increasing bulk susceptibility). Diamagnetic phases, such as quartz, have low-magnitude, slightly negative intrinsic susceptibilities that contribute little to the composite AMS signal if paramagnetic or ferromagnetic grains are present. Paramagnetic phases such as biotite have a moderately large positive susceptibility that will control the AMS if only diamagnetic and paramagnetic phases are present. The much higher intrinsic susceptibility of ferromagnetic grains (three orders of magnitude greater than paramagnetic phases) will dominate the signal when present (e.g., Hargraves et al., 1991; Grégoire et al., 1995).

The AMS signal of granite is commonly dominated by either paramagnetic (biotite and/or hornblende as the dominant magnetic phases) or ferromagnetic (magnetite and/or other iron

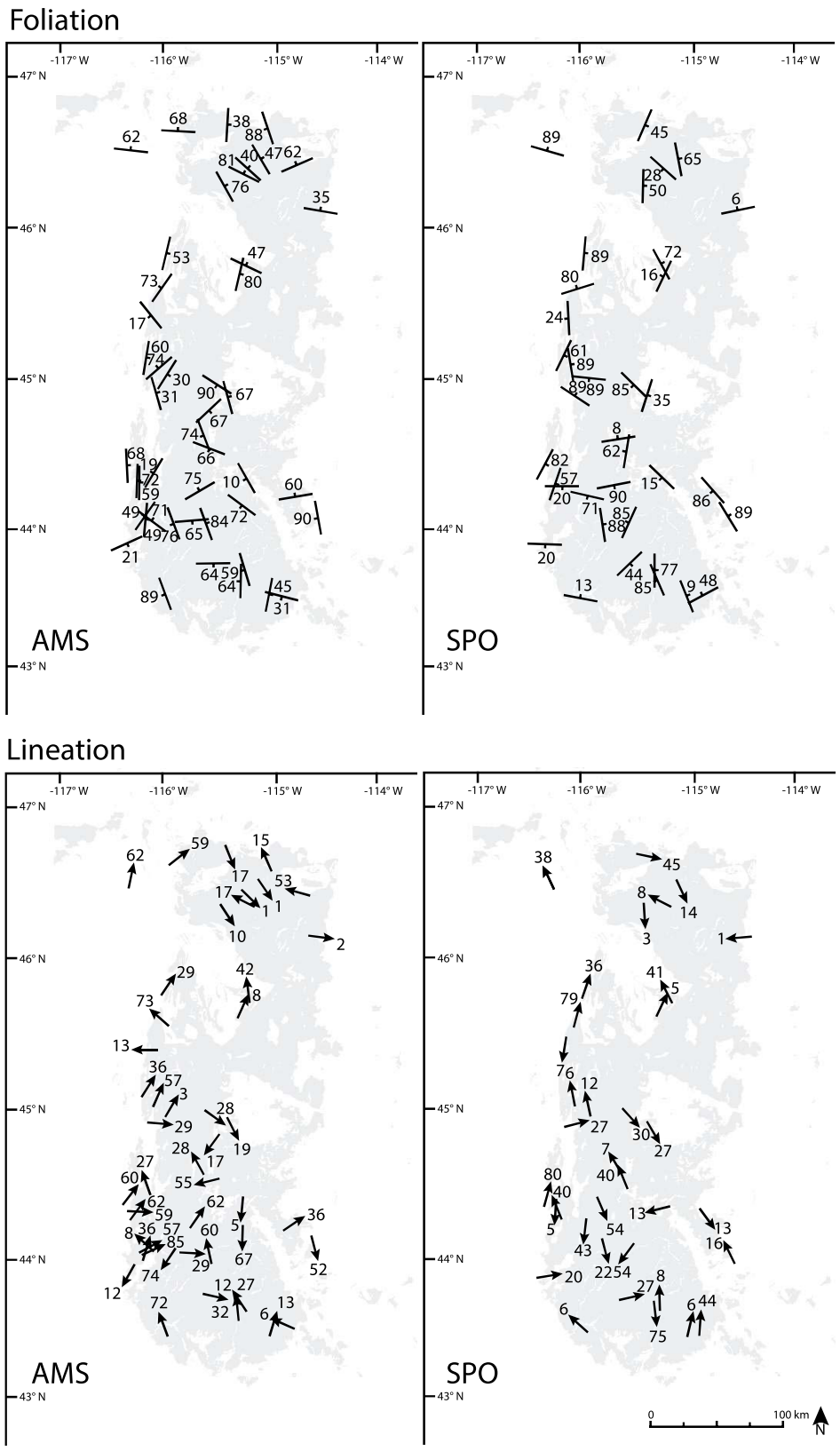

Figure 5. Foliation (above) and lineation (below) results from shape preferred orientation (SPO, right) and anisotropy of magnetic susceptibility (AMS, left) analyses. Foliation strikes consistently N-S in the border zone suite on the western boundary of the batholith. Foliation strikes consistently NW in the Bitterroot lobe. In the Atlanta lobe, fabric shows no trend in orientation. Lineations are highly variable, except in the Bitterroot peraluminous suite, where they are shallow to subhorizontal.

oxides as the dominant magnetic phase) minerals. The AMS signal in granitic rocks is due to either grain shape or crystallographic anisotropy. In paramagnetic materials, the crystallographic axes are parallel to the magnetic axes. In biotite, the crystallographic axes are also parallel to the shape axes. AMS fabrics formed by biotite grains, therefore, are a proxy for the grain SPO. AMS fabrics resulting from ferromagnetic grains may be due to either grain shape or grain distribution (e.g., Hargraves et al., 1991; Stephenson, 1994; Grégoire et al., 1995). The presence of single-domain ferromagnetic grains may result in magnetic interactions with each other during AMS analyses. In this case, the AMS ellipsoid may reflect an aggregate anisotropy rather than grain shape anisotropy (e.g., Bouchez, 1997). For all multidomain ferromagnetic materials, the AMS signal is controlled by grain shape. The aggregate AMS represents the average orientation and fabric shape of all of the magnetic grains (both ferromagnetic and paramagnetic) within the measured volume. Quantification of the degree and orientation of this anisotropy allows for rapid, nondestructive measurement of the average SPOs of grains within a sample.

Low-field AMS was measured for samples from 47 sites (42 of which correspond to SPO samples sites). AMS measurements were made at the University of Wisconsin–Madison on an AGICO KLY-3 Kappabridge magnetic susceptibility bridge. Between 5 and 10 specimens (1-in.-diameter core [2.54 cm]) prepared from at least three separate cores were analyzed from each site. Using AGICO Anisoft 4.2 software and the tensor statistical techniques of Jelínek and Kropáček (1978), susceptibility was determined for each of the three measurement axes, and data were combined into AMS ellipsoids.

Magnetic Characterization Methods

Magnetic characterization of the samples was carried out at the Institute for Rock Magnetism at the University of Minnesota, Twin Cities. Bulk susceptibility results from AMS analyses were used to select representative samples from each magmatic suite. Susceptibility versus temperature measurements were carried out on 17 samples (Fig. 6). For samples with high magnetic susceptibility, hysteresis measurements were performed (Fig. 7). Details of the analyses are given in Byerly (2014).

Magnetic Characterization Results

Results from high-temperature susceptibility measurements confirm the presence of a ferromagnetic phase in samples with high bulk magnetic susceptibility (Fig. 6). The early metaluminous and Bitterroot suite samples show a consistent magnetic unblocking temperature of ~575 °C, characteristic of magnetite (Fig. 6). Thus, the AMS signal from high-magnetic-susceptibility samples is controlled by ferromagnetic minerals. Some samples (Atlanta, late metaluminous suites) record a gradual change in susceptibility across the temperature range, indicative of paramagnetic mineralogy, but with a larger change at ~575 °C (see Byerly, 2014). For these samples, we interpret the AMS signal to be controlled by a paramagnetic component with a secondary ferromagnetic component.

Representative results of hysteresis measurements from high-magnetic-susceptibility samples are shown in Figure 7. Out of the 17 analyses, 16 contain multidomain magnetite, and one contains pseudo-single-domain magnetite (Fig. 8). These results suggest that multidomain magnetite will dominate the AMS signal, consistent with most magnetite-bearing granitic rocks (e.g., Uyeda et al., 1963; Bouchez, 1997). As such, we anticipate a direct correlation between magnetic and shape fabrics. For samples that were not characterized using these techniques, the bulk magnetic susceptibility determined during AMS measurements was used to classify samples in

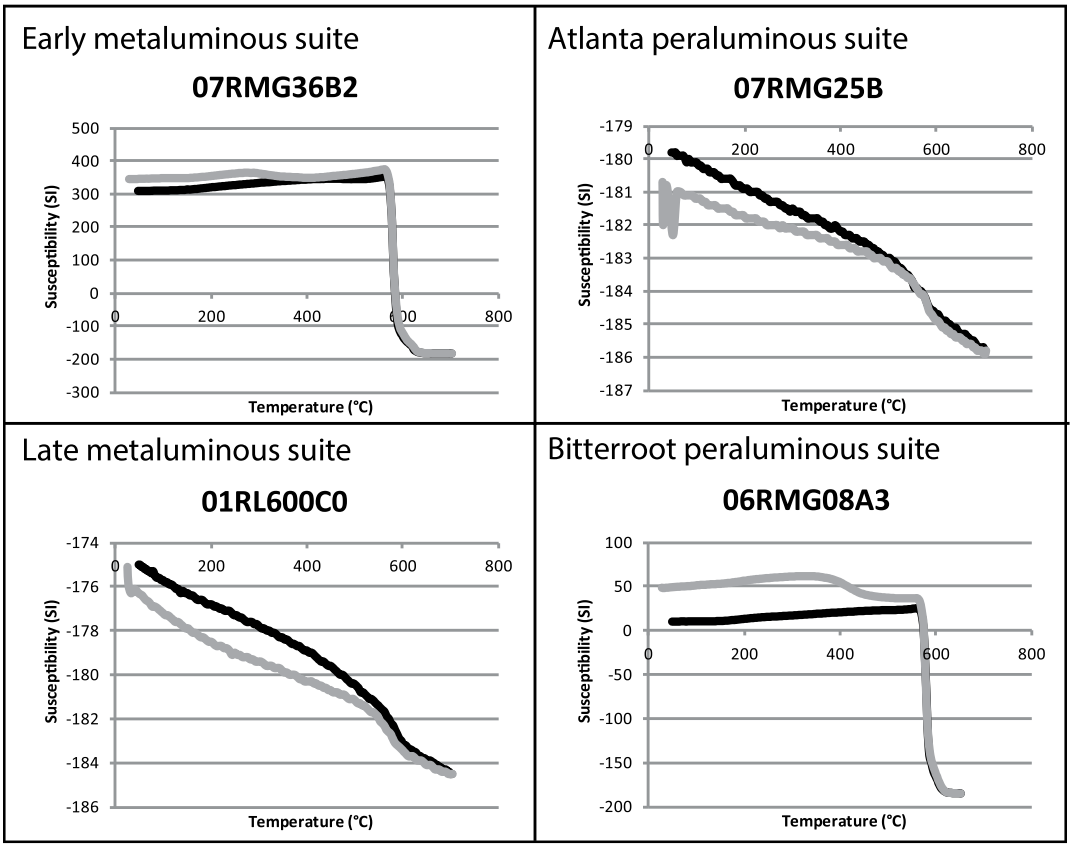

Figure 6. Representative hysteresis loops from a sample from each suite. The nonlinear hysteresis loops indicate a ferromagnetic component of the rock for the early metaluminous (and border zone) and Bitterroot peraluminous suites. Dominantly paramagnetic behavior occurs in Atlanta peraluminous and late metaluminous suites.

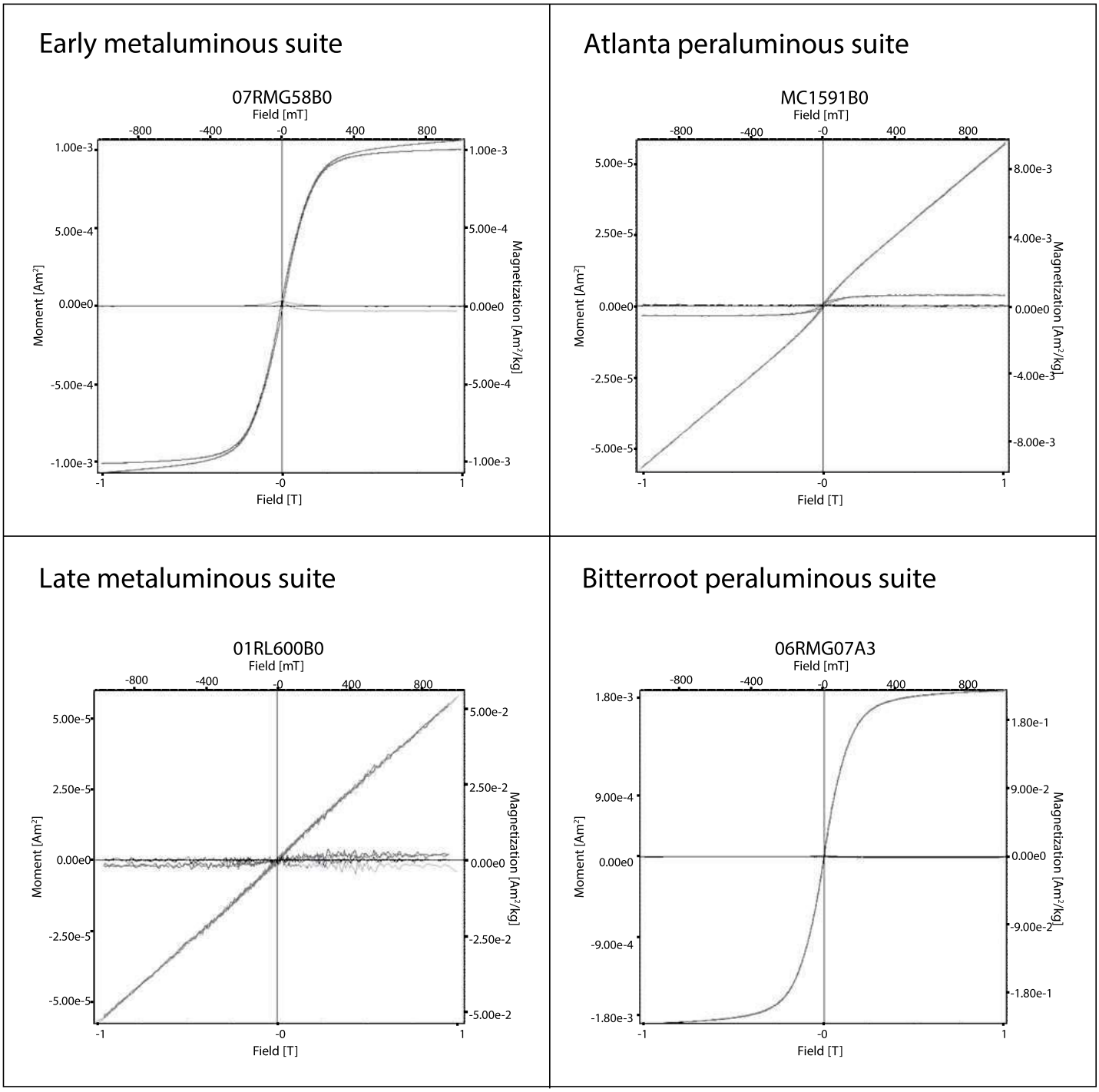

Figure 7. Representative magnetic susceptibility vs. temperature plots for a sample from each suite. Gray line is the heating curve; black line is the cooling curve. A dramatic decrease in magnetic susceptibility at ~575 °C indicates the presence of magnetite (a ferromagnetic mineral). The Atlanta peraluminous and late metaluminous suites contain some magnetite, but significantly less than the early metaluminous (and border zone) and Bitterroot peraluminous suites.

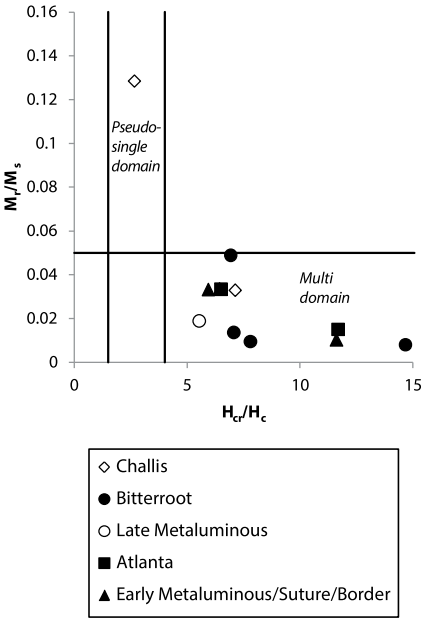

Figure 8. Day plot that allows evaluation of the domain state of ferromagnetic grains from samples in this study. The y-axis is remanent magnetization divided by saturation magnetization (M_r/M_s). The x-axis is coercivity of remanence over magnetic coercivity (H_{cr}/H_c). All samples, except one sample from the Challis suite, indicate the presence of multidomain magnetite.

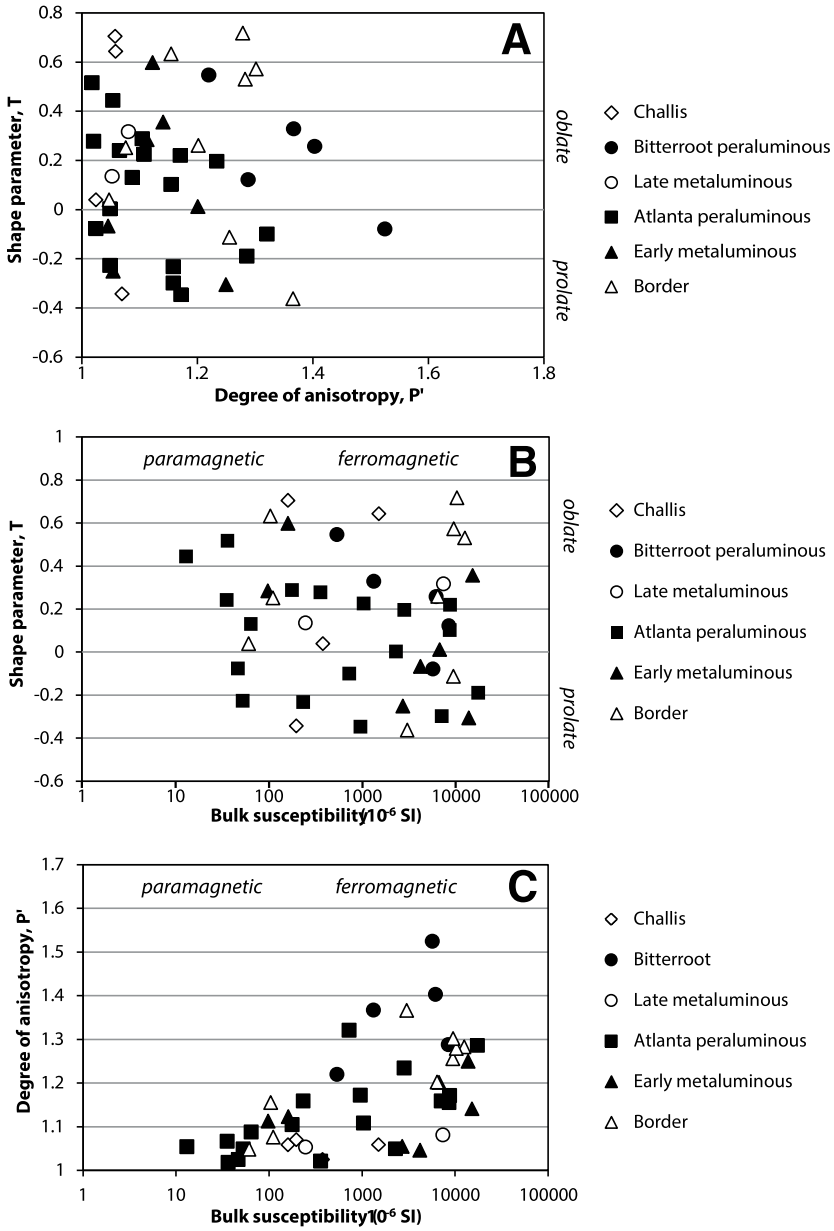

Figure 9. (A) Shape parameter vs. degree of anisotropy plot showing that fabric shape ranges from prolate to oblate regardless of fabric strength. (B) Shape parameter vs. bulk susceptibility plot showing that the class of magnetic material has little control over the shape of fabrics. Fabrics are dominantly oblate, though fabric shape is variable. (C) Degree of anisotropy vs. bulk susceptibility plot showing that there is a weak trend of increasing anisotropy with increasing bulk susceptibility. This is likely due to the higher intrinsic susceptibility of ferromagnetic phases such as magnetite.

the paramagnetic-dominant and ferromagnetic-dominant fields.

AMS Results

Bulk susceptibility of measured samples from the Idaho batholith ranges from 13 to 17,400 × 10^{-6} SI, with an average of 3724 × 10^{-6} SI (Fig. 9). The high bulk susceptibility indicates that the AMS signals of many granites are dominated by the ferromagnetic component. Only the early metaluminous (98–85 Ma) and Atlanta peraluminous (83–67 Ma) suites have sites that are dominated by the paramagnetic component. The degree of anisotropy (P′) ranges from 1.014 to 1.881. For all samples in this study, the shape parameter, T, ranges from –0.805 to 0.941, encompassing a wide range of fabric shapes. The average fabric shape is slightly oblate (Fig. 9).

The AMS fabrics of the suture zone and border zone suites exhibit N-S–oriented foliation with a steep E dip. These fabrics are similar to field measurements and fabrics determined using SPO analyses. The bulk magnetic susceptibility in these early phases of the batholith ranges from paramagnetic to ferromagnetic. Early metaluminous granites show no consistency in orientation. The corrected degree of anisotropy from AMS results ranges from 1.05 to 1.28. Fabric shapes are dominantly oblate, with a range of –0.36 to 0.72.

The fabrics measured using AMS in the Atlanta peraluminous suite are consistently very weak and highly variable in orientation (Figs. 5 and 9). Bulk susceptibility is variable across the Atlanta lobe, suggesting both ferromagnetic (eight samples) and paramagnetic (10 samples) minerals dominate the AMS signal. The corrected degree of anisotropy from AMS results ranges from 1.02 to 1.32. Fabric shapes are weakly prolate in the center of the suite, and oblate toward the margins. The shape parameter ranges from –0.35 to 0.52. The AMS foliation differs, in some cases, from the SPO foliation. In general, the mismatch is due to the presence of very weak fabrics, such that the two different

methods are recording small deviations from random fabric. In a few cases, the mismatch is due to large degrees of variation within a sample site, leading to a poorly constrained average AMS ellipsoid (samples 07RMG45 and 10RMG20).

Magnetic fabrics of the Bitterroot lobe depend on the intrusive suite, with the Bitterroot peraluminous suite having stronger and more consistently oriented AMS fabrics than the late metaluminous suite (Figs. 5 and 9). The two late metaluminous suite sites analyzed in this study have low-anisotropy (average 1.07), oblate fabrics. Foliation is consistent in the Bitterroot peraluminous suite, and AMS fabrics are in general agreement with field measurements and results from SPO measurements. AMS foliations consistently strike NW and dip to the NE, and measurements are consistent in the field, in AMS, and in SPO measurements. The degree of anisotropy from AMS results ranges from 1.22 to 1.53. Fabric shapes are dominantly oblate, with a shape parameter range of −0.08 to 0.52.

Figure 10 shows the variation in the AMS fabric through time. The AMS results are plotted using the degree of anisotropy (P′). The timing is constrained through the U-Pb zircon ages: The presence of magmatic microstructures and the relatively upper-crustal emplacement of the Idaho batholith allow us to assume that the crystallization age is approximately the time of fabric development. As such, we note that within the Idaho batholith, strong fabrics formed at two different periods. The first period occurred during emplacement of the border zone and early metaluminous suite, during or immediately after deformation in the western Idaho shear zone. The second period occurred during emplacement of the Bitterroot peraluminous belt.

$^{40}Ar/^{39}Ar$ THERMOCHRONOLOGY

Methodology

Three samples, previously dated for U-Pb zircon crystallization ages, were analyzed for $^{40}Ar/^{39}Ar$ closure ages to constrain the timing of the solid-state fabric development. Each sample was crushed, sieved, and separated for individual biotite phenocrysts. Biotite phenocrysts along with the 28.201 ± 0.046 Ma Fish Canyon tuff sanidine standard (Kuiper et al., 2008) were irradiated for 40 h at the Oregon State University TRIGA reactor in the Cadmium-Lined In-Core Irradiation Tube. Single biotite phenocrysts were incrementally heated using a 25 W CO_2 laser in the WiscAr Geochronology Laboratory. Gas cleanup and isotopic analysis using the MAP 215–50 mass spectrometer followed the methods of Jicha et al. (2006). The ages reported herein are shown with 2σ analytical uncertainties (including J uncertainty) and were calculated using the decay constants of Min et al. (2000).

Results

Suture Zone Suite

Sample 10RMG011 (Fig. 2) is a biotite-hornblende tonalite from within the western Idaho shear zone (Sage Hen orthogneiss of Braudy et al., 2016), with a zircon U-Pb age of 93.0 ± 3.4 Ma (Gaschnig et al., 2010). The biotite plateau $^{40}Ar/^{39}Ar$ was calculated to be 82.48 ± 0.24 Ma (Fig. 11). This cooling age is consistent with the results of Giorgis et al. (2008), which show cooling below $^{40}Ar/^{39}Ar$ closure temperatures in biotite between 85 and 70 Ma in the mylonites of the suture zone suite in the western Idaho shear zone. Samples in the suture zone suite record cooling from crystallization (~700 °C; Cherniak and Watson, 2001) through the ~350–400 °C closure temperature for argon in biotite (Grove and Harrison, 1996) in ~10 m.y., corresponding to an average cooling rate of ~35 °C/m.y.

Atlanta Peraluminous Suite

Sample 10RL896 (Fig. 2) is a granodiorite belonging to the Atlanta peraluminous suite (80–67 Ma) with a zircon U-Pb age of 71.9 ± 2.7 Ma (Gaschnig et al., 2016). The sample yielded a plateau biotite $^{40}Ar/^{39}Ar$ of 69.01 ± 0.22 Ma (Fig. 11). Sample 07RMG56 (Fig. 2) is a biotite granodiorite of the Atlanta peraluminous suite with a zircon U-Pb age of 76.3 ± 2.6 Ma. This sample yielded a younger biotite plateau $^{40}Ar/^{39}Ar$ age of 46.89 ± 0.15 Ma (Fig. 11).

Samples in the Atlanta peraluminous suite with similar crystallization ages yielded two very different average cooling rates: a rapid rate for 10RL896, between 86.0 °C/m.y. and nearly

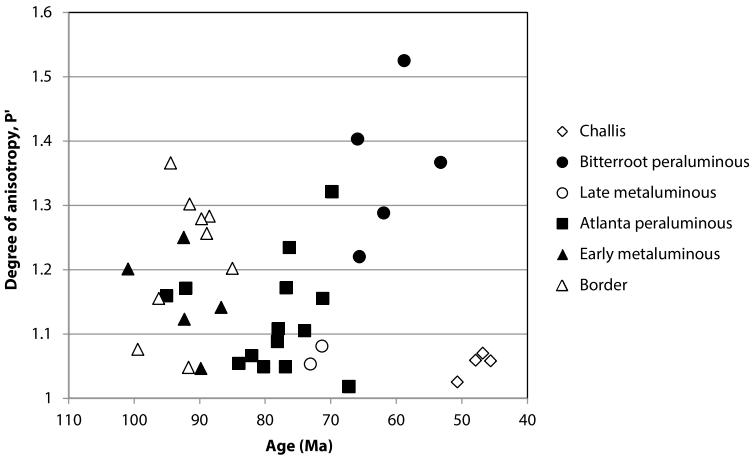

Figure 10. Plot of anisotropy of magnetic susceptibility (AMS) fabric strength through time. Fabrics in the Atlanta peraluminous suite (83–67 Ma) and the Challis intrusive suite (53–41 Ma) are consistently weak. The strongest fabrics are found in the border zone, early metaluminous, and Bitterroot peraluminous suites.

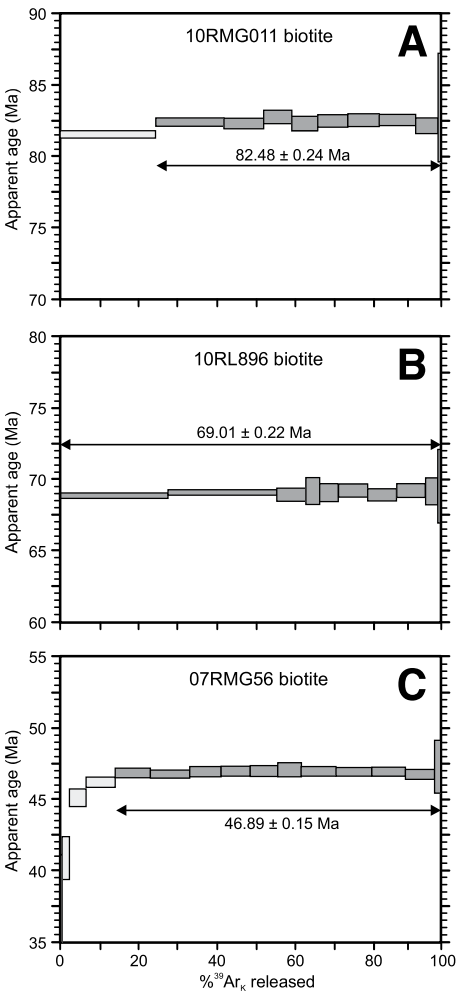

Figure 11. Three $^{40}Ar/^{39}Ar$ age spectrum diagrams for biotite phenocrysts. See text for details.

instantaneous cooling (average 173 °C/m.y.); and a slower (average 17 °C/m.y.) cooling rate for 07RMG56. The slower cooling rate may reflect the proximity of sample 07RMG56 to nearby intrusive Eocene Challis magmatism (Banner Creek stock; Fig. 2; Kiilsgaard et al., 2006). Rocks of the Atlanta peraluminous suite may have been reheated above closure temperatures for argon in biotite due to the influx of heat during later emplacement of Challis intrusives. The rapid cooling rate is likely more reflective of the overall pattern in the Atlanta peraluminous suite.

DISCUSSION

Constraints on Regional Tectonics during Construction of the Idaho Batholith

The integration of fabric data with existing zircon (U-Pb) and new biotite $^{40}Ar/^{39}Ar$ ages constrains timing of fabric development (Fig. 11). The zircon (U-Pb) and biotite $^{40}Ar/^{39}Ar$ ages give maximum and minimum ages of fabric development, respectively. The AMS and SPO thus record the deformational regime during the time period between zircon crystallization and cooling through the argon closure temperature in biotite.

Suture zone and border zone suites. The suture zone suite samples were affected by the western Idaho shear zone and are characterized by strong solid-state foliation. Fabrics measured using SPO and AMS in samples from these early plutons are strong, N-S–striking and E-dipping foliation and downdip lineation, consistent with field measurements (Fig. 12). The border zone suite shows similar fabrics. The ca. 91 Ma Payette River tonalite, a part of the border zone suite and located immediately east of the

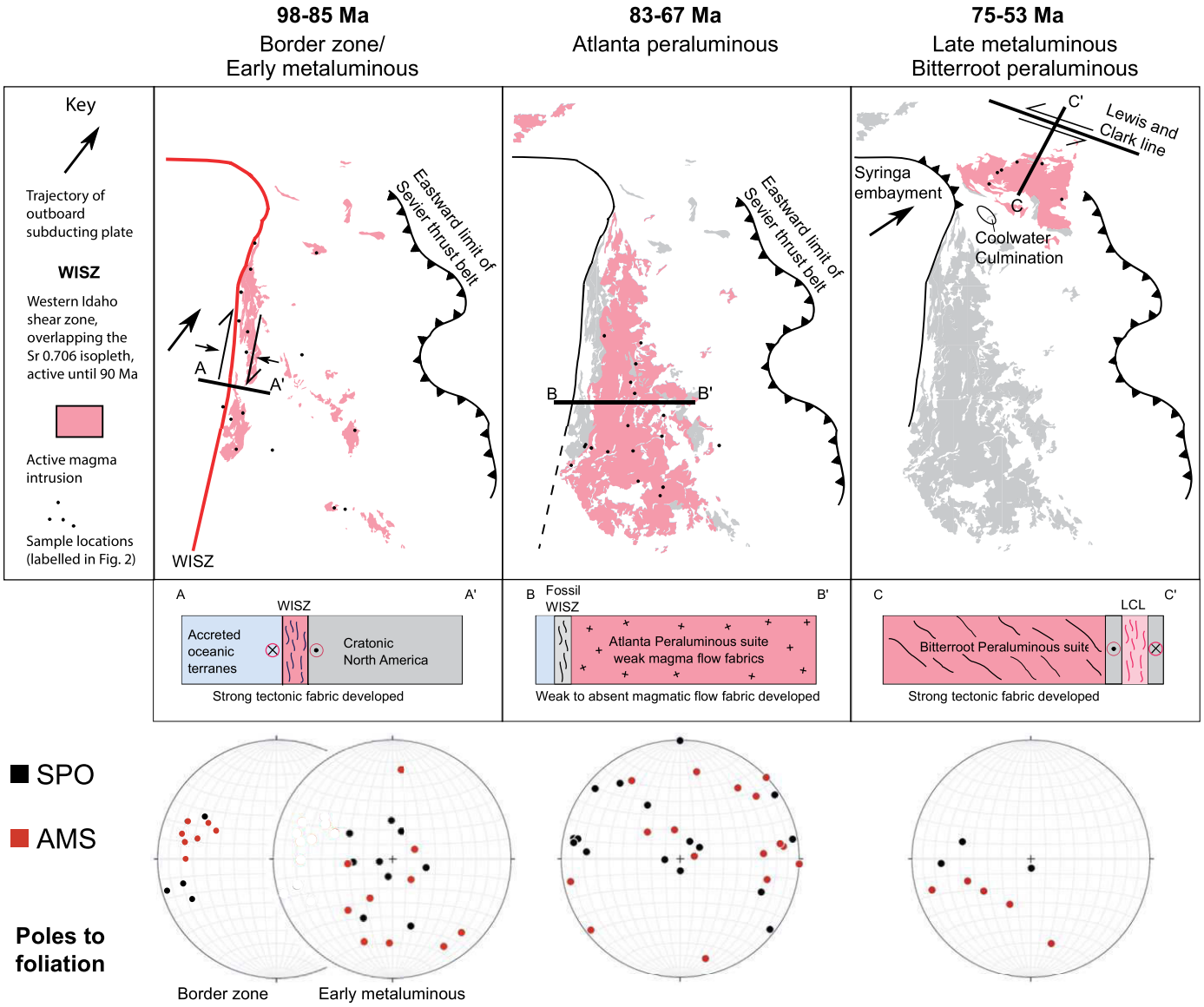

Figure 12. Tectonic evolution of the Idaho batholith, shown for different times (98–85 Ma, 83–67 Ma, and 75–53 Ma). Pink indicates location of active magmatism. Dark black line indicates the location of the cross section that characterizes the interaction between magmatism and tectonism for that time interval. Lower-hemisphere equal-area projections of the poles to foliation for shape preferred orientation (SPO) and anisotropy of magnetic susceptibility (AMS) results are given below. Early and late phases of the batholith record fabrics that formed due to regional strain. Fabrics in the Atlanta peraluminous suite are relatively weak. The sample locations are labeled in Figure 2. LCL—Lewis and Clark line.

western Idaho shear zone, records a N-S–striking fabric that grades eastward into a parallel magmatic fabric. Fabrics in this unit, therefore, resulted from waning western Idaho shear zone deformation that ceased at 90 Ma (Giorgis et al., 2008). In contrast, the younger metaluminous granites of the border zone suite exhibit N-S–striking foliation, parallel to the western Idaho shear zone fabrics, but they lack a consistent downdip lineation. We interpret these fabrics to result from continued regional contraction until 85 Ma (Giorgis et al., 2008).

Early metaluminous suite. The early metaluminous plutons (98–85 Ma) are found on the northern and eastern boundaries of the Atlanta lobe (Fig. 2) and as roof pendants and septa in younger batholith units. Fabrics measured in the early metaluminous plutons are weaker and are not parallel to the strong fabrics of the border zone suite (Fig. 12). Given that the ages of the early metaluminous suite plutons and the border zone suite plutons overlap, regional deformation at this time was likely partitioned. Transpressional deformation associated with the western Idaho shear zone may have been restricted to the western edge of the Idaho batholith.

Atlanta peraluminous suite. The 83–67 Ma Atlanta peraluminous suite is lithologically homogeneous and structurally isotropic at the outcrop scale. Magmatic microstructures are preserved in many samples, and solid-state overprinting, where present, is weak. Foliations in the Atlanta peraluminous suite show no consistent trend in orientation and no clear progression in fabric orientation through time, suggesting a lack of distributed regional deformation (Fig. 12). AMS results suggest generally a low degree of anisotropy and poorly constrained AMS ellipsoids. Further, fabric measurements for the same sample site differ in strength and orientation when comparing the AMS and SPO results. In summary, the granitoids of the Atlanta peraluminous suite appear isotropic.

The approximately N-S–trending Deadwood structure (Johnson Peak–Profile Gap shear zone of Lund, 2004) does occur within Atlanta lobe. Because the timing of deformation is presently unconstrained, we do not incorporate this zone into a model of Atlanta peraluminous suite development.

Due to the lack of pervasive and consistent deformation, we envision the fabrics of the Atlanta peraluminous suite to represent magma flow within a series of intrusions. Because there has been no significant subsolidus deformation, the magmatic structure of these individual intrusions has likely been preserved. The margins of the intrusions may also have been obliterated due to local remelting of intrusive contacts during intrusion of subsequent pulses of magma. Our interpretation of discrete, but obscured, individual plutons is consistent with the protracted growth history of the Atlanta peraluminous suite as evidenced by the ubiquitous and complexly zoned zircon grains analyzed in recent studies (Gaschnig et al., 2010, 2011).

Late metaluminous and Bitterroot peraluminous suites. Construction of the 75–53 Ma Bitterroot lobe exhibits a renewed cycle of low-volume metaluminous magmatism followed by higher-volume peraluminous magmatism. Only two samples were collected from the late metaluminous suite, and they have weak fabrics with orientations that are not consistent with nearby measurements (Fig. 12).

Fabrics in the Bitterroot peraluminous suite are some of the strongest in the batholith. Foliation strikes NW-SE, and lineations are shallowly plunging. Due to the consistency of foliation orientation, the higher degree of anisotropy, and the presence of some solid-state fabrics, we interpret the fabric of the Bitterroot peraluminous suite to represent distributed regional strain. This regional deformation—and the Bitterroot lobe itself—is limited to northern Idaho (e.g., Foster et al., 2001). Regional deformation did occur in northern Idaho at this time, as evidenced by movement on multiple, large-scale structures in the region, such as (1) the Lewis and Clark line, and (2) the Coolwater culmination (Wallace et al., 1990; Lund et al., 2008). The Lewis and Clark line is a WNW-ESE–trending zone of faults and shear zones that cuts through northern Idaho and western Montana (Wallace et al., 1990; Sears and Hendrix, 2004). Foliation orientations in the Bitterroot peraluminous suite are parallel to the Lewis and Clark line, which experienced sinistral transpression during the intrusion of the Bitterroot lobe (e.g., McClelland and Oldow, 2007). Contractional, NE-oriented deformation is also documented on the Coolwater culmination, to the southwest of the Bitterroot lobe, at this time (86–61 Ma) (Lund et al., 2008). The Coolwater culmination is interpreted to have formed by wedging of oceanic crust into the Syringa embayment (Fig. 2) on the margin of Laurentia, and this interpretation is consistent with NE-SW–directed shortening (Lund et al., 2008). Given the lack of evidence of deformation anywhere in the Atlanta lobe, Late Cretaceous–Paleogene strain appears to have been localized in the Syringa embayment (Schmidt et al., 2016).

85–70 Ma Orogenic Plateau in Idaho

It is difficult to account for the weak fabrics of the Atlanta peraluminous suite (Atlanta lobe) of the Idaho batholith. The Atlanta peraluminous suite was emplaced within a regional contractional regime, as evidenced by ongoing deformation in the Sevier fold-and-thrust belt to the east (e.g., Wiltschko and Dorr, 1983; DeCelles and Mitra, 1995). With the degree of shortening attributed to the Sevier orogeny—an estimated 220 km of shortening occurred on the Sevier fold-and-thrust belt (DeCelles and Coogan, 2006)—we would expect to see strong tectonically imparted fabrics, both magmatic and solid state, in the voluminous Atlanta peraluminous intrusive suite.

The Atlanta lobe of the Idaho batholith likely intruded into a crustal plateau. A fault restoration model by Coney and Harms (1984) shows that the Cordilleran crust was up to 60 km thick in central Idaho. This finding is consistent with recent seismic data (K. Davenport, 2016, personal commun.), which constrain the current depth of the Moho to 37–40 km below current exposure levels in the Atlanta lobe of the Idaho batholith. Using the 3–4 kbar emplacement pressures for the exposed early metaluminous suite (98–85 Ma; Gaschnig et al., 2010), based on the Al-in-hornblende geobarometer (Jordan, 1994), the maximum emplacement depth for the Atlanta peraluminous suite is ~12 km. The geophysical and geobarometry data together constrain the thickness of the Idaho batholith to be ~50 km during emplacement of the Atlanta suite. This crustal plateau is also consistent with central Idaho being a major sediment source for Late Cretaceous paleorivers draining to basins in California, Wyoming, and Washington (e.g., Dumitru et al., 2016).

The Atlanta lobe is part of a continent-scale two-mica granite belt that is immediately inboard of the other North American Cordilleran batholiths (Fig. 1; Miller and Bradfish, 1980). The belt stretches ~1300 km from Arizona to Canada and is evidenced by 41 muscovite-bearing, dominantly quartz monzonite or granitic plutonic units. These rocks have generally high silica (>70%) and high $^{87}Sr/^{86}Sr$ (0.7086–0.734), indicating a more peraluminous composition than the Cordilleran arc batholiths (Miller and Bradfish, 1980). The Idaho batholith is the greatest contiguous volume in this discontinuous belt. The geochemical data from the Atlanta peraluminous suite are consistent with the interpretation of emplacement in overthickened crust (Gaschnig et al., 2011). The zircons from the Atlanta peraluminous suite display extensive inheritance and multiple generations of Cretaceous growth (Gaschnig et al., 2010, 2016), in addition to Precambrian inheritance (Gaschnig et al., 2013). The evolved Nd and Hf isotopes imply only limited, if any, mantle input (Gaschnig et al., 2011). Together, these data suggest large-scale crustal melting, which we interpret to have been caused by crustal thickening. In contrast, the other Cordilleran arc batholiths

(e.g., Sierra Nevada, Coast plutonic complex, Peninsular Range) have more voluminous mafic components, and the granitoids are dominantly metaluminous, suggesting contribution of juvenile mantle material (e.g., Bateman, 1992; Todd et al., 1998; McNulty et al., 2000; Ortega-Rivera, 2003; Gehrels et al., 2009).

The weak fabrics of the Atlanta peraluminous suite can potentially be explained by emplacement in a crustal plateau. The crustal thickening required to generate a plateau may lead to contrasting styles of deformation within an orogen. In overthickened crust, a vertical gradient can develop in lithospheric deformation, transitioning from contraction at the plateau roots to extension in the upper crust, with an intervening plane of neutrality (Molnar and Lyon-Caen, 1988; Rey et al., 2001). Crustal thickening in the Andean and Himalayan plateaus has been shown to lead to gravitational instability, resulting in extensional accommodation in the upper crust (e.g., Hodges et al., 1992; Flesch and Kreemer, 2010). The lack of strong tectonic fabric in the Atlanta peraluminous suite suggests that the current exposure level may reflect this transition between contraction and extension (Fig. 12). This interpretation accounts for ongoing shortening in the foreland as a product of lateral variations in gravitational potential energy (e.g., Molnar and Lyon-Caen, 1988).

The difficulty with this interpretation is that the level of neutral extension only extends a limited distance down from the surface of a crustal plateau. The depth of the transition is given by z = horizontal stress/(density × gravitational acceleration) (Molnar and Lyon-Caen, 1988). For density = 2700 kg/m^3 and gravitational acceleration = 9.8 m/s^2, this equation becomes horizontal stress/26,460 Pa. Estimates for horizontal stress from crustal plateaus are 25 MPa (Peruvian Andes; Richardson and Coblentz, 1994), 7–10 MPa (Himalaya; Panthi, 2012), 4–25 MPa (eastern margin of the Tibetan Plateau; Meng et al., 2015), and −10 to 20 MPa (eastern margin of the Tibetan Plateau; Styron and Hetland, 2015). Assuming a horizontal stress of 20 MPa, the depth where vertical stress is equal to horizontal stress ("neutral" stress) is ~755 m. However, Copley et al. (2009) suggested that if mountains were supported by the ductile part of the lithosphere (e.g., lithospheric mantle), then stresses of 80–240 MPa are supported. If so, the depth of "neutral" stress is ~3–9 km. Thus, it is permissive that upper-crustal magmatism in a crustal plateau could occur in a neutral environment.

An alternative model is that the magmas of the Atlanta lobe were intruded as thin, horizontal sheets. This mode of emplacement has been documented in mafic-silicic layered intrusions studied by R. Wiebe and colleagues based on exposures in Maine, United States (e.g., Wiebe, 1993; Wiebe and Collins, 1998). Horizontal layering has since been recognized in dominantly silicic systems (Miller and Miller, 2002; Harper et al., 2004; Waight et al., 2007). Further, individual intrusive horizontal sheets have been recognized in the shallow (<5 km depth) silicic intrusions of the Henry Mountains, Utah (e.g., Horsman et al., 2005; Morgan et al., 2008). The lack of clear plutonic boundaries in the Atlanta lobe of the Idaho batholith is permissive of this geometry. Each of these magma sheets would crystallize and cool in a geologically short (~10^5 yr) period of time at upper-crustal (<10 km) depths (e.g., Nyman et al., 1995). As such, these magma sheets, which are relatively viscous, may not record regional contraction in a manner similar to a larger pluton. A difficulty with this model is that ductile shear zones are commonly reported from the margins of thin, fast-cooling meter-scale tabular intrusions (Féménias et al., 2004; Horsman et al., 2005; Creixell et al., 2006).

We cannot discriminate between these two options, or the possibility of their simultaneous operation, as the cause of the ubiquitous weak fabrics recorded in the Atlanta lobe. In order to fully evaluate these scenarios, sampling and geochronologic, microstructural, and fabric analysis would need to be done at a much finer spatial scale.

CONCLUSIONS

The Idaho batholith consists of series of intrusive suites (Gaschnig et al., 2010) that exhibit distinctive variations in fabric development. We were able to constrain the orientation and magnitude of tectonic strain through time within the batholith, because the granites: (1) record dominantly magmatic fabrics; (2) cooled relatively quickly (~3 m.y.) through ~350 °C as constrained by ^{40}Ar/^{39}Ar closure ages on biotite; and (3) have crystallization ages known from U-Pb zircon analyses (Gaschnig et al., 2010, 2013; Braudy et al., 2016). Fabrics in the suture and border suites, on the western margin of the Idaho batholith, were affected by Late Cretaceous deformation associated with the western Idaho shear zone. These fabrics are typically N-S oriented and show solid-state to slightly solid-state microstructures. The Atlanta peraluminous suite, despite being emplaced during orogenesis, records very weak and randomly oriented fabrics, and it contains only magmatic microstructures. The Bitterroot peraluminous suite exhibits strong and regionally consistent NW-oriented fabrics, with some solid-state microstructures. In general, the SPO fabrics determined from biotite and the AMS fabrics are consistent throughout the Idaho batholith, with the exception of the weakly developed fabrics in the Atlanta peraluminous suite. The lack of strong fabrics in the voluminous Atlanta peraluminous suite, in combination with the crustal thickness estimates and geochemical analyses, is consistent with emplacement in an orogenic plateau and/or sill-like emplacement.

ACKNOWLEDGMENTS

We thank Michael Kedenburg and Joey Lane for their help as field assistants for A. Byerly. C.E. Bate and N. Garibaldi are gratefully acknowledged for help with revisions. We thank three anonymous reviews whose comments significantly improved the quality of the manuscript. This work was supported by National Science Foundation grants EAR-0844260 and EAR-1251877 to B. Tikoff (University of Wisconsin–Madison).

REFERENCES CITED

Aranguren, A., Tubia, J., Bouchez, J.L., and Vigneresse, J.L., 1996, The Guitiriz granite, Variscan belt of northern Spain: Extension-controlled emplacement of magma during tectonic escape: Earth and Planetary Science Letters, v. 139, p. 165–176, doi:10.1016/0012-821X(95)00239-9.

Archanjo, C., and Campanha, G., 2012, Using AMS combined with mineral shape preferred orientation analysis to understand the emplacement fabrics of the Apiaí gabbro-norite (Ribeira belt, SE Brazil): International Journal of Earth Sciences, v. 101, p. 731–745, doi:10.1007/s00531-011-0659-x.

Archanjo, C.J., Launeau, P., and Bouchez, J.L., 1995, Magnetic fabric vs. magnetite and biotite shape fabrics of the magnetite-bearing granite pluton of Gameleiras (northeast Brazil): Physics of the Earth and Planetary Interiors, v. 89, p. 63–75, doi:10.1016/0031-9201(94)02997-P.

Archanjo, C.J., da Silva, E.R., and Caby, R., 1999, Magnetic fabric and pluton emplacement in a transpressive shear zone system: The Itaporanga porphyritic granitic pluton (northeast Brazil): Tectonophysics, v. 312, p. 331–345, doi:10.1016/S0040-1951(99)00176-6.

Archanjo, C.J., Hollanda, M.H.B.M., Rodrigues, S.W.O., Neves, B.B.B., and Armstrong, R., 2008, Fabrics of pre- and syntectonic granite plutons and chronology of shear zones in the Eastern Borborema Province, NE Brazil: Journal of Structural Geology, v. 30, p. 310–326, doi:10.1016/j.jsg.2007.11.011.

Armstrong, R.L., Taubeneck, W.H., and Hales, P.O., 1977, Rb-Sr and K-Ar geochronometry of Mesozoic granitic rocks and their Sr isotopic composition, Oregon, Washington, and Idaho: Geological Society of America Bulletin, v. 88, p. 397–411, doi:10.1130/0016-7606(1977)88<397.

Bateman, P., 1992, Plutonism in the Central Part of the Sierra Nevada Batholith, California: U.S. Geological Survey Professional Paper 1483, 186 p.

Baxter, S., Graham, N.T., Feely, M., Reavy, R.J., and Dewey, J.F., 2005, A microstructural and fabric study of the Galway Granite, Connemara, western Ireland: Geological Magazine, v. 142, p. 81–95, doi:10.1017/S0016756804000378.

Benn, K., 2010, Anisotropy of magnetic susceptibility fabrics in syntectonic plutons as tectonic strain markers: The example of the Canso pluton, Meguma terrane, Nova Scotia, *in* Clemens, J.D., and Donaldson, C., eds., Sixth Hutton Symposium on the Origin of Granites and Related Rocks: Geological Society of America Special Paper 472, p. 147–158, doi:10.1017/S1755691009016028.

Benn, K., Horne, R.J., Kontak, D.J., Pignotta, G.S., and Evans, N.G., 1997, Syn-Acadian emplacement model for the South Mountain batholith, Meguma terrane, Nova Scotia: Magnetic fabric and structural analyses: Geological Society of America Bulletin, v. 109, p. 1279–1293, doi:10.1130/0016-7606(1997)109<1279.

Benn, K., Ham, N.M., Pignotta, G.S., and Bleeker, W., 1998, Emplacement and deformation of granites during transpression: Magnetic fabrics of the Archean Sparrow pluton, Slave Province, Canada: Journal of Structural Geology, v. 20, p. 1247–1259, doi:10.1016/S0191-8141(98)00065-0.

Benn, K., Roest, W.R., Rochette, P., Evans, N.G., and Pignotta, G.S., 1999, Geophysical and structural signatures of

syntectonic batholith construction: The South Mountain batholith, Meguma terrane, Nova Scotia: Geophysical Journal International, v. 136, p. 144–158, doi:10.1046/j.1365-246X.1999.00700.x.

Benn, K., Paterson, S.R., Lund, S.P., Pignotta, G.S., and Kruse, S., 2001, Magmatic fabrics in batholiths as markers of regional strains and plate kinematics: Example of the Cretaceous Mt. Stuart batholith: Physics and Chemistry of the Earth, ser. A, Solid Earth and Geodesy, v. 26, p. 343–354, doi:10.1016/S1464-1895(01)00064-3.

Blumenfeld, P., and Bouchez, J.L., 1988, Shear criteria in granite and migmatite deformed in the magmatic and solid states: Journal of Structural Geology, v. 10, p. 361–372, doi:10.1016/0191-8141(88)90014-4.

Borradaile, G.J., and Henry, B., 1997, Tectonic applications of magnetic susceptibility and its anisotropy: Earth-Science Reviews, v. 42, p. 49–93, doi:10.1016/S0012-8252(96)00044-X.

Borradaile, G.J., and Jackson, M., 2004, Anisotropy of magnetic susceptibility (AMS): Magnetic petrofabrics of deformed rocks, *in* Martín-Hernández, F., Lüneburg, C.M., Aubourg, C., and Jackson, M., eds., Magnetic Fabric: Methods and Applications: Geological Society, London, Special Publication 238, p. 299–360, doi:10.1144/GSL.SP.2004.238.01.18.

Bouchez, J., 1997, Granite is never isotropic: An introduction to AMS studies of granitic rocks, *in* Bouchez, J., Hutton, D.H.W., and Stephens, W.E., eds., Granite: From Segregation of Melt to Emplacement Fabrics: Dordrecht, Netherlands, Kluwer Academic Publishers, p. 95–112.

Bouchez, J.L., and Gleizes, G., 1995, Two-stage deformation of the Mont-Louis-Andorra granite pluton (Variscan Pyrenees) inferred from magnetic susceptibility anisotropy: Journal of the Geological Society, London, v. 152, p. 669–679, doi:10.1144/gsjgs.152.4.0669.

Bouchez, J.L., Gleizes, G., Djouadi, T., and Rochette, P., 1990, Microstructure and magnetic susceptibility applied to emplacement kinematics of granites: The example of the Foix pluton (French Pyrenees): Tectonophysics, v. 184, p. 157–171, doi:10.1016/0040-1951(90)90051-9.

Braudy, N., Gaschnig, R.M., Wilford, D., Vervoort, J.D., Nelson, C.L., Davidson, C., Kahn, M.J., and Tikoff, B., 2016, Timing and deformation conditions of the western Idaho shear zone, West Mountain, west-central Idaho: Lithosphere, doi:10.1130/L519.1 (in press).

Brun, J.P., and Pons, J., 1981, Strain patterns of pluton emplacement in a crust undergoing non-coaxial deformation, Sierra Morena: Southern Spain: Journal of Structural Geology, v. 3, p. 219–229, doi:10.1016/0191-8141(81)90018-3.

Brun, J.P., Gapais, D., Cogne, J.P., Ledru, P., and Vigneresse, J.L., 1990, The Flamanville Granite (northwest France): An unequivocal example of a syntectonically expanding pluton: Geological Journal, v. 25, p. 271–286, doi:10.1002/gj.3350250310.

Byerly, A., 2014, Tectonic History of the Idaho Batholith; Fabric Analysis through Time [M.S. thesis]: Madison, Wisconsin, University of Wisconsin–Madison, 96 p.

Cao, W., Paterson, S., Memeti, V., Mundil, R., Anderson, J.L., and Schmidt, K., 2015, Tracking paleodeformation fields in the Mesozoic central Sierra Nevada arc: Implications for intra-arc cyclic deformation and arc tempos: Lithosphere, v. 7, p. 296–320, doi:10.1130/L389.1.

Chardon, D., Andronicos, C.L., and Hollister, L.S., 1999, Large-scale transpressive shear zone patterns and displacements within magmatic arcs: The Coast plutonic complex, British Columbia: Tectonics, v. 18, p. 278–292, doi:10.1029/1998TC900035.

Cherniak, D.J., and Watson, E.B., 2001, Pb diffusion in zircon: Chemical Geology, v. 172, p. 5–24, doi:10.1016/S0009-2541(00)00233-3.

Coney, P.J., and Harms, T.A., 1984, Cordilleran metamorphic core complexes: Cenozoic extensional relics of Mesozoic compression: Geology, v. 12, p. 550, doi:10.1130/0091-7613(1984)12<550:CMCCCE>2.0.CO;2.

Copley, A., Boait, F., Hollingsworth, J., Jackson, J., and McKenzie, D., 2009, Subparallel thrust and normal faulting in Albania and the roles of gravitational potential energy and rheology contrasts in mountain belts: Journal of Geophysical Research, v. 114, p. B05407, doi:10.1029/2008JB005931.

Creixell, C., Parada, M., Roperch, P., Morata, D., Arriagada, C., and De Arce, C., 2006, Syntectonic emplacement of the Middle Jurassic Concon mafic dike swarm, Coastal Range, central Chile: Tectonophysics, v. 425, p. 101–122, doi:10.1016/j.tecto.2006.07.005.

Cruden, A., and Launeau, P., 1994, Structure, magnetic fabric and emplacement of the Archean Lebel Stock, SW Abitibi greenstone belt: Journal of Structural Geology, v. 16, p. 677–691, doi:10.1016/0191-8141(94)90118-X.

DeCelles, P.G., and Coogan, J.C., 2006, Regional structure and kinematic history of the Sevier fold-and-thrust belt, central Utah: Geological Society of America Bulletin, v. 118, p. 841–864, doi:10.1130/B25759.1.

DeCelles, P.G., and Mitra, G., 1995, History of the Sevier orogenic wedge in terms of critical taper models, northeast Utah and southwest Wyoming: Geological Society of America Bulletin, v. 107, p. 454–462, doi:10.1130/0016-7606(1995)107<0454.

DeCelles, P.G., Ducea, M.N., Kapp, P., and Zandt, G., 2009, Cyclicity in Cordilleran orogenic systems: Nature Geoscience, v. 2, p. 251–257, doi:10.1038/ngeo469.

de Saint-Blanquat, M., Law, R.D., Bouchez, J.-L., and Morgan, S.S., 2001, Internal structure and emplacement of the Papoose Flat pluton: An integrated structural, petrographic, and magnetic susceptibility study: Geological Society of America Bulletin, v. 113, p. 976–995, doi:10.1130/0016-7606(2001)113<0976.

de Saint-Blanquat, M., Habert, G., Horsman, E., Morgan, S.S., Tikoff, B., Launeau, P., and Gleizes, G., 2006, Mechanisms and duration of non-tectonically assisted magma emplacement in the upper crust: The Black Mesa pluton, Henry Mountains, Utah: Tectonophysics, v. 428, p. 1–31, doi:10.1016/j.tecto.2006.07.014.

Dumitru, T.A., Elder, W.P., Hourigan, J.K., Chapman, A.D., Graham, S.A., and Wakabayashi, J., 2016, Four Cordilleran paleorivers that connected Sevier thrust zones in Idaho to depocenters in California, Washington, Wyoming, and, indirectly, Alaska: Geology, v. 44, p. 75–78, doi:10.1130/G37286.1.

Féménias, O., Diot, H., Berza, T., Gauffriau, A., and Demaiffe, D., 2004, Asymmetrical to symmetrical magnetic fabric of dikes: Paleo-flow orientations and paleo-stresses recorded on feeder-bodies from the Motru dike swarm (Romania): Journal of Structural Geology, v. 26, p. 1401–1418, doi:10.1016/j.jsg.2003.12.003.

Ferré, E., Wilson, J., and Gleizes, G., 1999, Magnetic susceptibility and AMS of the Bushveld alkaline granites, South Africa: Tectonophysics, v. 307, p. 113–133, doi:10.1016/S0040-1951(99)00122-5.

Flesch, L.M., and Kreemer, C., 2010, Gravitational potential energy and regional stress and strain rate fields for continental plateaus: Examples from the central Andes and Colorado Plateau: Tectonophysics, v. 482, p. 182–192, doi:10.1016/j.tecto.2009.07.014.

Foster, D.A., Schafer, C., Fanning, C.M., and Hyndman, D.W., 2001, Relationships between crustal partial melting, plutonism, orogeny, and exhumation: Idaho–Bitterroot batholith: Tectonophysics, v. 342, p. 313–350, doi:10.1016/S0040-1951(01)00169-X.

Fowler, T.K., and Paterson, S.R., 1997, Timing and nature of magmatic fabrics from structural relations around stoped blocks: Journal of Structural Geology, v. 19, p. 209–224, doi:10.1016/S0191-8141(96)00058-2.

Gaschnig, R.M., Vervoort, J.D., Lewis, R.S., and McClelland, W.C., 2010, Migrating magmatism in the northern US Cordillera: In situ U-Pb geochronology of the Idaho batholith: Contributions to Mineralogy and Petrology, v. 159, p. 863–883, doi:10.1007/s00410-009-0459-5.

Gaschnig, R.M., Vervoort, J.D., Lewis, R.S., and Tikoff, B., 2011, Isotopic evolution of the Idaho batholith and Challis intrusive province, northern US Cordillera: Journal of Petrology, v. 52, p. 2397–2429, doi:10.1093/petrology/egr050.

Gaschnig, R.M., Vervoort, J.D., Lewis, R.S., and Tikoff, B., 2013, Probing for Proterozoic and Archean crust in the northern US Cordillera with inherited zircon from the Idaho batholith: Geological Society of America Bulletin, v. 125, p. 73–88, doi:10.1130/B30583.1.

Gaschnig, R., Vervoort, J., Tikoff, B., and Lewis, R.S., 2016, Construction and preservation of batholiths in the northern US Cordillera: Lithosphere, doi:10.1130/L497.1 (in press).

Gehrels, G., Rusmore, M., Woodsworth, G., Crawford, M., Andronicos, C., Hollister, L., Patchett, J., Ducea, M., Butler, R., Klepeis, K., and Davidson, C., 2009, U-Th-Pb geochronology of the Coast Mountains batholith in north-coastal British Columbia: Constraints on age and tectonic evolution: Geological Society of America Bulletin, v. 121, p. 1341–1361, doi:10.1130/B26404.1.

Giorgis, S., McClelland, W.C., Fayon, A.K., Singer, B.S., and Tikoff, B., 2008, Timing of deformation and exhumation in the western Idaho shear zone, McCall, Idaho: Geological Society of America Bulletin, v. 120, p. 1119–1133, doi:10.1130/B26291.1.

Gleizes, G., Leblanc, D., Santana, V., Olivier, P., and Bouchez, J.L., 1998, Sigmoidal structures featuring dextral shear during emplacement of the Hercynian granite complex of Cauterets–Panticosa (Pyrenees): Journal of Structural Geology, v. 20, p. 1229–1245, doi:10.1016/S0191-8141(98)00060-1.

Grégoire, V., Saint Blanquat, M., Nedelec, A., and Bouchez, J.-L., 1995, Shape anisotropy versus magnetic interactions of magnetite grains: Experiments and application of AMS in granitic rocks: Geophysical Research Letters, v. 22, p. 2765–2768, doi:10.1029/95GL02797.

Grove, M., and Harrison, T.M., 1996, $^{40}Ar^{*}$ diffusion in Fe-rich biotite: The American Mineralogist, v. 81, p. 940–951, doi:10.2138/am-1996-7-816.

Gutiérrez, F., Payacán, I., Gelman, S.E., Bachmann, O., and Parada, M.A., 2013, Late-stage magma flow in a shallow felsic reservoir: Merging the anisotropy of magnetic susceptibility record with numerical simulations in La Gloria pluton, central Chile: Journal of Geophysical Research–Solid Earth, v. 118, p. 1984–1998, doi:10.1002/jgrb.50164.

Hargraves, R.B., Johnson, D., and Chan, C.Y., 1991, Distribution anisotropy: The cause of AMS in igneous rocks: Geophysical Research Letters, v. 18, p. 2193–2196, doi:10.1029/91GL01777.

Harper, B.E., Miller, C.F., Koteas, G.C., Gates, N.L., Wiebe, R.A., Lazzareschi, D.S., and Cribb, J.W., 2004, Granites, dynamic magma chamber processes and pluton construction: The Aztec Wash pluton, Eldorado Mountains, Nevada, USA, *in* Ishihara, S., Stephens, W.E., Harley, S.L., Arima, M., and Nakajima, T., eds., The Fifth Hutton Symposium on the Origin of Granitic and Related Rocks: Geological Society of America Special Paper 389, p. 277–295, doi:10.1130/0-8137-2389-2.277.

Henry, B., Liégeois, J., Nouar, O., and Derder, M., 2009, Repeated granitoid intrusions during the Neoproterozoic along the western boundary of the Saharan metacraton, Eastern Hoggar, Tuareg shield, Algeria: An AMS and U-Pb zircon age study: Tectonophysics, v. 474, p. 417–434, doi:10.1016/j.tecto.2009.04.022.

Hirth, G., and Tullis, J., 1992, Dislocation creep regimes in quartz aggregates: Journal of Structural Geology, v. 14, p. 145–159, doi:10.1016/0191-8141(92)90053-Y.

Hodges, K.V., Parrish, R.R., Housh, T.B., Lux, D.R., Burchfiel, B.C., Royden, L.H., and Chen, Z., 1992, Simultaneous Miocene extension and shortening in the Himalayan orogen: Science, v. 258, no. 5087, p. 1466–1470, doi:10.1126/science.258.5087.1466.

Horsman, E., Tikoff, B., and Morgan, S.S., 2005, Emplacement-related fabric and multiple sheets in the Maiden Creek sill, Henry Mountains, Utah, USA: Journal of Structural Geology, v. 27, p. 1426–1444, doi:10.1016/j.jsg.2005.03.003.

Hrouda, F., 1982, Magnetic anisotropy of rocks and its application in geology and geophysics: Geophysical Surveys, v. 5, p. 37–82, doi:10.1007/BF01450244.

Hutton, D.H.W., 1988, Granite emplacement mechanisms and tectonic controls: Inferences from deformation studies: Royal Society of Edinburgh Transactions: Earth Science, v. 79, p. 245–255.

Jelínek, V., 1981, Characterization of the magnetic fabric of rocks: Tectonophysics, v. 79, p. 63–67, doi:10.1016/0040-1951(81)90110-4.

Jelínek, V., and Kropáček, V., 1978, Statistical processing of anisotropy of magnetic susceptibility measured on groups of specimens: Studia Geophysica et Geodaetica, v. 22, p. 50–62, doi:10.1007/BF01613632.

Jicha, B.R., Scholl, D.W., Singer, B.S., Yogodzinski, G.M., and Kay, S.M., 2006, Revised age of Aleutian Island arc formation implies high rate of magma production: Geology, v. 34, p. 661–664, doi:10.1130/G22433.1.

Jordan, B., 1994, Emplacement and Exhumation of the Southeastern Atlanta Lobe of the Idaho Batholith and Outlying Stocks, South Central Idaho [M.S. thesis]: Pocatello, Idaho, Idaho State University, 110 p.

Karlstrom, K., Miller, C. F., Kingsbury, J. A., and Wooden, J. L., 1993, Pluton emplacement along an active ductile thrust zone, Piute Mountains, southeastern California: Interaction between deformational and solidification processes: Geological Society of America Bulletin, 105, no. 2, p. 213–230, doi:10.1130/0016-7606(1993)105<0213.

Kiilsgaard, T.H., Stanford, L.R., and Lewis, R.S., 2006, Geologic Map of the Deadwood River 30 × 60 Minute Quadrangle, Idaho: Idaho Geological Survey Geologic Map 45, scale 1:100,000.

Kuiper, K., Deino, A., Hilgen, F., Krijgsman, W., Renne, P., and Wijbrans, J., 2008, Synchronizing rock clocks of Earth history: Science, v. 320, p. 500–504, doi:10.1126/science.1154339.

Launeau, P., and Cruden, A., 1998, Magmatic fabric acquisition mechanisms in a syenite: Results of a combined anisotropy of magnetic susceptibility and image analysis study: Journal of Geophysical Research, v. 103, p. 5067–5089, doi:10.1029/97JB02670.

Launeau, P., and Robin, P., 1996, Fabric analysis using the intercept method: Tectonophysics, v. 267, p. 91–119, doi:10.1016/S0040-1951(96)00091-1.

Launeau, P., Bouchez, J.-L., and Benn, K., 1990, Shape preferred orientation of object populations: Automatic analysis of digitized images: Tectonophysics, v. 180, p. 201–211, doi:10.1016/0040-1951(90)90308-U.

Leblanc, D., Gleizes, G., Roux, L., and Bouchez, J.L., 1996, Variscan dextral transpression in the French Pyrenees: New data from the Pit des Trois-Seigneurs granodiorite and its country rocks: Tectonophysics, v. 261, p. 331–345, doi:10.1016/0040-1951(95)00174-3.

Lloyd, G.E., and Freeman, B., 1994, Dynamic recrystallization of quartz under greenschist conditions: Journal of Structural Geology, v. 16, p. 867–881, doi:10.1016/0191-8141(94)90151-1.

Lund, K., Snee, L., and Evans, K., 1986, Age and genesis of precious metals deposits, Buffalo Hump District, central Idaho; implications for depth of emplacement of quartz veins: Economic Geology and the Bulletin of the Society of Economic Geologists, v. 81, p. 990–996, doi:10.2113/gsecongeo.81.4.990.

Lund, K., 2004, Geology of the Payette National Forest and Vicinity, West-Central Idaho: U.S. Geological Survey Professional Paper 1666, 89 p.

Lund, K., Aleinikoff, J., and Yacob, E., 2008, Coolwater culmination: Sensitive high-resolution ion microprobe (SHRIMP) U/Pb and isotopic evidence for continental delamination in the Syringa: Tectonics, v. 27, TC2009, doi:10.1029/2006TC002071.

Majumder, S., and Mamtani, M.A., 2009, Magnetic fabric in the Malanjkhand Granite (central India)—Implications for regional tectonics and Proterozoic suturing of the Indian Shield: Physics of the Earth and Planetary Interiors, v. 172, p. 310–323, doi:10.1016/j.pepi.2008.10.007.

Mamtani, M.A., and Greiling, R.O., 2005, Granite emplacement and its relation with regional deformation in the Aravalli Mountain Belt (India)—Inferences from magnetic fabric: Journal of Structural Geology, v. 27, p. 2008–2029, doi:10.1016/j.jsg.2005.06.004.

Mamtani, M.A., Pal, T., and Greiling, R.O., 2013, Kinematic analysis using AMS data from a deformed granitoid: Journal of Structural Geology, v. 50, p. 119–132, doi:10.1016/j.jsg.2012.03.002.

Manduca, C.A., Silver, L.T., and Tayor, H.P., 1992, $^{87}Sr/^{86}Sr$ and $^{18}O/^{16}O$ isotopic systematics and geochemistry of granitoid plutons across a steeply-dipping boundary between contrasting lithospheric blocks in western Idaho: Contributions to Mineralogy and Petrology, v. 109, p. 355–372, doi:10.1007/BF00283324.

Manduca, C.A., Kuntz, M.E.L.A., and Silver, L.T., 1993, Emplacement and deformation history of the western margin of the Idaho batholith near McCall, Idaho: Influence of a major terrane boundary: Geological Society of America Bulletin, v. 105, p. 749–765, doi:10.1130/0016-7606(1993)105<0749.

Marre, J., 1986, The Structural Analysis of Granitic Rocks: New York, Elsevier, 123 p.

McClelland, W.C., and Oldow, J.S., 2007, Late Cretaceous truncation of the western Idaho shear zone in the central North American Cordillera: Geology, v. 35, p. 723–726, doi:10.1130/G23623A.1.

McNulty, B.A., Tobisch, O.T., Cruden, A.R., and Gilder, S., 2000, Multistage emplacement of the Mount Givens pluton, central Sierra Nevada batholith, California: Geological Society of America Bulletin, v. 112, p. 119–135, doi:10.1130/0016-7606(2000)112<119.

Mecklenburgh, J., and Rutter, E., 2003, On the rheology of partially molten synthetic granite: Journal of Structural Geology, v. 25, p. 1575–1585, doi:10.1016/S0191-8141(03)00014-2.

Meng, W., Chen, Q., Zhao, Z., Wu, M., Qin, X., and Zhang, C., 2015, Characteristics and implications of the stress state in the Longmen Shan fault zone, eastern margin of the Tibetan Plateau: Tectonophysics, v. 656, p. 1–19, doi:10.1016/j.tecto.2015.04.010.

Miller, C.F., and Bradfish, L.J., 1980, An inner Cordilleran belt of muscovite-bearing plutons: Geology, v. 8, p. 412–416, doi:10.1130/0091-7613(1980)8<412.

Miller, C.F., and Miller, J.S., 2002, Contrasting stratified plutons exposed in tilt blocks, Eldorado Mountains, Colorado River Rift, NV, USA: Lithos, v. 61, p. 209–224, doi:10.1016/S0024-4937(02)00080-4.

Min, K., Mundil, R., Renne, P.R., and Ludwig, K.R., 2000, A test for systematic errors in $^{40}Ar/^{39}Ar$ geochronology through comparison with U/Pb analysis of a 1.1-Ga rhyolite: Geochimica et Cosmochimica Acta, v. 64, p. 73–98, doi:10.1016/S0016-7037(99)00204-5.

Molnar, P., and Lyon-Caen, H., 1988, Some simple physical aspects of the support, structure, and evolution of mountain belts, *in* Clark, S.P., Jr., Burchfield, B.C., and Suppe, J., eds., Processes in Continental Lithosphere Deformation: Geological Society of America Special Paper 218, p. 179–208, doi:10.1130/SPE218-p179.

Morgan, S.S., Stanik, A., Horsman, E., Tikoff, B., St. Blanquat, M., and Habert, G., 2008, Emplacement of multiple magma sheets and wall rock deformation: Trachyte Mesa intrusion, Henry Mountains, Utah: Journal of Structural Geology, v. 30, p. 491–512, doi:10.1016/j.jsg.2008.01.005.

Morgan, S.S., Law, R., and de Saint Blanquat, M., 2013, Forceful emplacement of the Eureka Valley–Joshua Flat–Beer Creek composite pluton into a structural basin in eastern California: Internal structure and wall rock deformation: Tectonophysics, v. 608, p. 753–773, doi:10.1016/j.tecto.2013.08.003.

Naibert, T.J., Geissman, J.W., and Heizler, M.T., 2010, Magnetic fabric, paleomagnetic, and $^{40}Ar/^{39}Ar$ geochronologic data bearing on the emplacement of the Late Cretaceous Philipsburg Batholith, SW Montana fold-and-thrust belt: Lithosphere, v. 2, p. 303–327, doi:10.1130/L83.1.

Neves, S., Araújo, A., Correia, P., and Mariano, G., 2003, Magnetic fabrics in the Cabanas Granite (NE Brazil): Interplay between emplacement and regional fabrics in a dextral transpressive regime: Journal of Structural Geology, v. 25, p. 441–453, doi:10.1016/S0191-8141(02)00003-2.

Nyman, M.W., Law, R.D., and Morgan, S.S., 1995, Conditions of contact metamorphism, Papoose Flat pluton, eastern California, USA: Implications for cooling and strain histories: Journal of Metamorphic Geology, v. 13, p. 627–643, doi:10.1111/j.1525-1314.1995.tb00247.x.

Ortega-Rivera, A., 2003, Geochronological constraints on the tectonic history of the Peninsular Ranges batholith of Alta and Baja California: Tectonic implications for western México, *in* Johnson, S.E., Paterson, S.R., Fletcher, J.M., Girty, G.H., Kimbrough, D.L., and Martín-Barajas, A., eds., of Northwestern Mexico and the Southwestern USA: Geological Society of America Special Paper 374, p. 297–335, doi:10.1130/0-8137-2374-4.297.

Panthi, K.K., 2012, Evaluation of rock bursting phenomena in a tunnel in the Himalayas: Bulletin of Engineering Geology and the Environment, v. 71, p. 761–769, doi:10.1007/s10064-012-0444-5.

Parada, M.A., Roperch, P., Guiresse, C., and Ramírez, E., 2005, Magnetic fabrics and compositional evidence for the construction of the Caleu pluton by multiple injections, Coastal Range of central Chile: Tectonophysics, v. 399, p. 399–420, doi:10.1016/j.tecto.2004.12.032.

Paterson, S.R., and Ducea, M.N., 2015, Arc magmatic tempos; gathering the evidence: Elements, v. 11, p. 91–98, doi:10.2113/gselements.11.2.91.

Paterson, S.R., Vernon, R., and Tobisch, O., 1989, A review of criteria for the identification of magmatic and tectonic foliations in granitoids: Journal of Structural Geology, v. 11, p. 349–363, doi:10.1016/0191-8141(89)90074-6.

Paterson, S.R., Fowler, T.K., Schmidt, K.L., Yoshinobu, A.S., Yuan, E.S., and Miller, R.B., 1998, Interpreting magmatic fabric patterns in plutons: Lithos, v. 44, p. 53–82, doi:10.1016/S0024-4937(98)00022-X.

Pignotta, G.S., and Benn, K., 1999, Magnetic fabric of the Barrington Passage pluton, Meguma terrane, Nova Scotia: A two-stage fabric history of syntectonic emplacement: Tectonophysics, v. 307, p. 75–92, doi:10.1016/S0040-1951(99)00119-5.

Rey, P., Vanderhaeghe, O., and Teyssier, C., 2001, Gravitational collapse of the continental crust: Definition, regimes and modes: Tectonophysics, v. 342, p. 435–449, doi:10.1016/S0040-1951(01)00174-3.

Richardson, R.M., and Coblentz, D.D., 1994, Stress modeling in the Andes: Constraints on the South American intraplate stress magnitudes: Journal of Geophysical Research, v. 99, no. B11, p. 22,015–22,025, doi:10.1029/94JB01751.

Rosenberg, C.L., and Handy, M.R., 2005, Experimental deformation of partially melted granite revisited: Implications for the continental crust: Journal of Metamorphic Geology, v. 23, p. 19–28, doi:10.1111/j.1525-1314.2005.00555.x.

Sant'Ovaia, H., Olivier, P., and Ferreira, N., 2010, Magmatic structures and kinematics emplacement of the Variscan granites from central Portugal (Serra da Estrela and Castro Daire areas): Journal of Structural Geology, v. 32, p. 1450–1465, doi:10.1016/j.jsg.2010.09.003.

Schmidt, K.L., Lewis, R.S., Vervoort, J., Stetson-Lee, T.A., Michels, Z.D., and Tikoff, B., 2016, Tectonic evolution of the Syringa embayment in the central North American Cordilleran accretionary boundary: Lithosphere, doi:10.1130/L545.1 (in press).

Sears, J., and Hendrix, M., 2004, Lewis and Clark line and the rotational origin of the Alberta and Helena salients, North American Cordillera, *in* Sussman, A.J., and Weil, A.B., eds., Orogenic Curvature: Integrating Paleomagnetic and Structural Analyses: Geological Society of America Special Paper 383, p. 173–186.

Sen, K., and Mamtani, M.A., 2006, Magnetic fabric, shape preferred orientation and regional strain in granitic rocks: Journal of Structural Geology, v. 28, p. 1870–1882, doi:10.1016/j.jsg.2006.07.005.

Sen, K., Majumder, S., and Mamtani, M.A., 2005, Degree of magnetic anisotropy as a strain intensity gauge in ferromagnetic granites: Journal of the Geological Society, London, v. 162, p. 583–586, doi:10.1144/0016-764904-144.

Stephenson, A., 1994, Distribution anisotropy: Two simple models for magnetic lineation and foliation: Physics of the Earth and Planetary Interiors, v. 82, p. 49–53, doi:10.1016/0031-9201(94)90101-5.

Stevenson, C.T.E., Owens, W.H., and Hutton, D.H.W., 2007, Flow lobes in granite: The determination of magma flow direction in the Trawenagh Bay Granite, northwestern Ireland, using anisotropy of magnetic susceptibility: Geological Society of America Bulletin, v. 119, p. 1368–1386, doi:10.1130/B25970.1.

Stipp, M., Stunitz, H., Heilbronner, R., and Schmid, S.M., 2002, The eastern Tonale fault zone: A "natural laboratory" for crystal plastic deformation of quartz over a temperature range from 250 to 700 °C: Journal of Structural Geology, v. 24, p. 1861–1884, doi:10.1016/S0191-8141(02)00035-4.

Styron, R.H., and Hetland, E.A., 2015, The weight of the mountains: Constraints on tectonic stress, friction, and fluid pressure in the 2008 Wenchuan earthquake from estimates of topographic loading: Journal of Geophysical Research–Solid Earth, v. 120, p. 2697–2716, doi:10.1002/2014JB011338.

Tarling, D., and Hrouda, F., eds., 1993, Magnetic Anisotropy of Rocks: London, Chapman & Hall, 218 p.

Tobisch, O.T., and Cruden, A.R., 1995, Fracture-controlled magma conduits in an obliquely convergent continental magmatic arc: Geology, v. 23, p. 941–944, doi:10.1130/0091-7613(1995)023<0941.

Tobisch, O.T., Saleeby, J.B., Renne, P.R., McNulty, B., and Tong, W., 1995, Variations in deformation fields during development of a large-volume magmatic arc, central Sierra Nevada, California: Geological Society of America Bulletin, v. 107, p. 148–166, doi:10.1130/0016-7606(1995)107<0148.

Todd, V.R., Erskine, B.G., and Morton, D.M., 1998, Metamorphic and tectonic evolution of the northern Peninsular Ranges batholith, *in* Ernst, W.G., ed., Metamorphism and Crustal Evolution of the western United States: Rubey Volume VII: Englewood Cliffs, New Jersey, Prentice-Hall, p. 894–937.

Uyeda, S., Fuller, M.D., Belshé, J.C., and Girdler, R.W., 1963, Anisotropy of magnetic susceptibility of rocks and minerals: Journal of Geophysical Research, v. 68, p. 279–291, doi:10.1029/JZ068i001p00279.

Unruh, D.M., Lund, K., Snee, L.W., and Kuntz, M.A., 2008, Uranium-lead zircon ages and Sr, Nd, and Pb isotope geochemistry of selected plutonic rocks from western Idaho: U.S. Geological Survey Open-File Report 2008-1142, 42 p.

Vigneresse, J.L., and Tikoff, B., 1999, Strain partitioning during partial melting and crystallizing felsic magmas: Tectonophysics, v. 312, p. 117–132, doi:10.1016/S0040-1951(99)00167-5.

Waight, T.E., Wiebe, R.A., and Krogstad, E.J., 2007, Isotopic evidence for multiple contributions to felsic magma chambers: Gouldsboro Granite, coastal Maine: Lithos, v. 93, p. 234–247, doi:10.1016/j.lithos.2006.03.066.

Wallace, C.A., Lidke, D.J., and Schmidt, R.G., 1990, Faults of the central part of the Lewis and Clark line and fragmentation of the Late Cretaceous foreland basin in west-central Montana: Geological Society of America Bulletin, v. 102, p. 1021–1037, doi:10.1130/0016-7606(1990)102<1021.

Wiebe, R.A., 1993, The Pleasant Bay layered gabbro-diorite, coastal Maine: Ponding and crystallization of basaltic injections into a silicic magma chamber: Journal of Petrology, v. 34, p. 461–489, doi:10.1093/petrology/34.3.461.

Wiebe, R.A., and Collins, W.J., 1998, Depositional features and stratigraphic sections in granitic plutons: Implications for the emplacement and crystallization of granitic magma: Journal of Structural Geology, v. 20, p. 1273–1289, doi:10.1016/S0191-8141(98)00059-5.

Wiltschko, D.V., and Dorr, J.A., 1983, Timing of deformation in overthrust belt and foreland of Idaho, Wyoming, and Utah: American Association of Petroleum Geologists Bulletin, v. 67, p. 1304–1322, doi:10.1306/03B5B740-16D1-11D7-8645000102C1865D.

Yoshinobu, A.S., Okaya, D.A., and Paterson, S.R., 1998, Modeling the thermal evolution of fault-controlled magma emplacement models: Implications for the solidification of granitoid plutons: Journal of Structural Geology, v. 20, p. 1205–1218, doi:10.1016/S0191-8141(98)00064-9.

Zak, J., Paterson, S.R., and Memeti, V., 2007, Four magmatic fabrics in the Tuolumne batholith, central Sierra Nevada, California (USA): Implications for interpreting fabric patterns in plutons and evolution of magma chambers in the upper crust: Geological Society of America Bulletin, v. 119, p. 184–201, doi:10.1130/B25773.1.

MANUSCRIPT RECEIVED 12 APRIL 2016
REVISED MANUSCRIPT RECEIVED 30 JUNE 2016
MANUSCRIPT ACCEPTED 11 AUGUST 2016

Printed in the USA